

Algorithmically Designed Artificial Neural Networks (ADANNs): Higher order deep operator learning for parametric partial differential equations

Arnulf Jentzen^{1,2}, Adrian Riekert³, and Philippe von Wurstemberger^{4,5}

¹ School of Data Science and Shenzhen Research Institute of Big Data, The Chinese University of Hong Kong, Shenzhen (CUHK-Shenzhen), China; e-mail: ajentzen@cuhk.edu.cn

² Applied Mathematics: Institute for Analysis and Numerics, University of Münster, Germany; e-mail: ajentzen@uni-muenster.de

³ Applied Mathematics: Institute for Analysis and Numerics, University of Münster, Germany; e-mail: ariekert@uni-muenster.de

⁴ School of Data Science, The Chinese University of Hong Kong, Shenzhen (CUHK-Shenzhen), China; e-mail: philippevw@cuhk.edu.cn

⁵ Risklab, Department of Mathematics, ETH Zurich, Switzerland; e-mail: philippe.vonwurstemberger@math.ethz.ch

May 30, 2024

Abstract

In this article we propose a new deep learning approach to approximate operators related to parametric partial differential equations (PDEs). In particular, we introduce a new strategy to design specific artificial neural network (ANN) architectures in conjunction with specific ANN initialization schemes which are tailor-made for the particular approximation problem under consideration. In the proposed approach we combine efficient classical numerical approximation techniques with deep operator learning methodologies. Specifically, we introduce customized adaptations of existing ANN architectures together with specialized initializations for these ANN architectures so that at initialization we have that the ANNs closely mimic a chosen efficient classical numerical algorithm for the considered approximation problem. The obtained ANN architectures and their initialization schemes are thus strongly inspired by numerical algorithms as well as by popular deep learning methodologies from the literature and in that sense we refer to the introduced ANNs in conjunction with their tailor-made initialization schemes as *Algorithmically Designed Artificial Neural Networks* (ADANNs). We numerically test the proposed ADANN methodology in the case of several parametric PDEs. In the tested numerical examples the ADANN methodology significantly outperforms existing traditional approximation algorithms as well as existing deep operator learning methodologies from the literature.

Keywords: Deep learning, operator learning, parametric partial differential equations, numerical analysis, scientific computing.

Contents

1	Introduction	2
2	Overview of the ADANN methodology	5
2.1	Base model with highly specialized initializations	5
2.2	Difference models	6
2.3	Optimization over base model initializations	7
2.4	Pseudocode description of the ADANN methodology	7
3	Derivation of a base model for semilinear heat PDEs	9
3.1	One-dimensional semilinear heat PDEs	9
3.2	Designing algorithms for the base model	9
3.2.1	Spatial finite difference discretization	9
3.2.2	Temporal linearly implicit Runge-Kutta (LIRK) discretizations	10
3.2.3	A compact reformulation of the designing algorithms	10
3.3	Designing the base model and its initializations	11
4	Numerical simulations	11
4.1	Black box optimizers	12
4.1.1	Grid-based black box optimizer	12
4.1.2	Heuristic exploration-exploitation black box optimizer	12
4.2	Sine-Gordon-type equation	13
4.2.1	Base model for the Sine-Gordon-type equation	14
4.2.2	Numerical results for the one-dimensional Sine-Gordon-type equation	15
4.2.3	Numerical results for the two-dimensional Sine-Gordon-type equation	19
4.3	Viscous Burgers equation	22
4.3.1	Base model for the viscous Burgers equation	22
4.3.2	Numerical results for the viscous Burgers equation	23
4.4	Reaction diffusion equation	26
4.4.1	Base model for the reaction diffusion equation	26
4.4.2	Numerical results for the reaction diffusion equation	27
5	Conclusion and future work	28
	Appendix A Training	30
A.1	Optimal choice of initial learning rates	30
A.2	Adaptive reduction of learning rates	30
	Appendix B Second order LIRK methods	32
B.1	Order conditions for general LIRK methods	32
B.2	A family of 2 stage LIRK methods of order 2	33
B.3	The special case of the Crank–Nicolson explicit midpoint method	33

1 Introduction

Deep learning approximation methods – usually consisting of deep *artificial neural network* (ANN) models trained through *Stochastic Gradient Descent* (SGD) optimization methods – are nowadays among the most heavily employed approximation methods in the digital world. They are behind most of the recent success in artificial intelligence and machine learning in areas such as computer vision (cf., e.g. [20, 55, 92] and the references therein), natural language processing (cf., e.g., [12, 72, 76, 80, 91] and the references therein), and speech recognition (cf., e.g., [17, 41, 66, 94] and the references therein) and are increasingly used in many other fields. One such field is scientific computing where in recent years deep learning technologies have been intensively applied to various problems including to the numerical approximation of *partial differential equations* (PDEs).

In particular, deep learning approximation methods have been developed to approximately solve high-dimensional nonlinear PDEs (see, e.g., [5, 8, 22, 23, 29, 34, 47, 85] and the references therein) such as high-dimensional nonlinear pricing problems from financial engineering and Hamiltonian–Jacobi–Bellman equations from optimal control. In the context of such high-dimensional nonlinear PDEs the progress achieved by deep learning approximation methods is obvious as there are – except in some special cases (see, e.g., [39, 40, 69] and the references therein for Branching-type methods and see, e.g., [23–25, 46] and the references therein for multilevel Picard methods) – essentially no practical alternative numerical approximation methods. The striking feature of deep learning methods in the context of such high-dimensional problems is that in many situations numerical simulations suggest that the computational effort of such methods only grows at most polynomially in the input dimension of the problem under consideration. In contrast, classical numerical methods usually suffer under the so-called *curse of dimensionality* (cf., e.g., [7], [70, Chapter 1], and [71, Chapter 9]) in the sense that the computational effort grows at least exponentially in the dimension.

There is also a vast literature on deep learning approximation methods for low-dimensional PDEs (cf., e.g., [5, 47, 49, 77] and the references therein). For low-dimensional PDEs in most cases, there usually already exist a number of efficient classical (non-deep learning based) approximation methods in the scientific literature (cf., e.g., [4, 48, 57, 87]). Nonetheless, there are several convincing arguments that deep learning approximation methods might have the potential to significantly outperform such traditional approximation methods from classical numerics. One situation where this strongly applies is in the context of *parametric PDE* approximation problems. Specifically, in applications one is often not only interested in approximately solving a PDE model once but instead there is often the need to approximately solve a PDE model repeatedly but with different initial values and/or different model parameters. The idea of deep learning approaches in this context is to try to not only solve one fixed PDE but instead to learn the whole solution operator which maps initial values and model parameters to corresponding PDE solutions. Even though the original PDE model has often only one to three space-dimensions, the associated approximation problem for the solution operator typically becomes very high-dimensional due to the high number of parameters required to approximately describe the initial value and the model parameters. Because of their apparent capacity to overcome the curse of dimensionality, deep learning methods, therefore seem to be very natural candidates for such approximation problems. Deep learning methods in this situation are then often referred to as (*deep*) *operator learning* approaches (cf., e.g., [59, 60, 63]). However, even though very remarkable advances have been accomplished in this area of research, for instance, by means of so-called *Fourier neural operators* (FNOs) (see [60]), so far in most situations deep operator learning techniques do not outperform the most efficient higher order classical numerical methods. This is also not entirely surprising due to fundamental lower bounds established in the literature that a wide class of methods, including typical deep learning approximations, can in general not overcome the curse of dimensionality in the L^∞ -norm (cf., e.g., [31, 36, 37]).

It is precisely the objective of this work to introduce a new operator learning approach which aims to overcome this challenge by combining efficient classical numerical methods with deep operator learning techniques. In particular, we introduce a new strategy to design specific ANN architectures in conjunction with specific ANN initialization schemes which are tailor-made for the particular approximation problem under consideration. The obtained ANN architectures and their initialization schemes are strongly inspired by numerical algorithms as well as by popular deep learning methodologies from the literature and in that sense we refer to the introduced ANN architectures in conjunction with their tailor-made initialization schemes as *Algorithmically Designed Artificial Neural Networks* (ADANNs). We numerically test the ADANN methodology proposed in this paper in the case of several parametric PDEs. In the tested numerical examples the ADANN methodology significantly outperforms classical approximation algorithms as well as existing deep operator learning methodologies from the literature.

We now briefly describe some key aspects of the ADANN methodology proposed in this paper in more detail. Roughly speaking, the architecture of ADANNs consists of two components: a *base model* and a *difference model*. Given a family of efficient classical numerical algorithms for a considered approximation problem, a base model is designed together with highly specialized initializations for that model such that at those initializations the base model exactly represents the considered efficient classical numerical algorithms. Such a base model is trained to approximate the considered target operator using SGD-type methods starting at its highly specialized initializations. Loosely speaking, the training of a base model

can be seen as improving the classical numerical algorithms. On the other hand, a difference model can be chosen to be any operator learning model from the literature and is trained to approximate the difference between the target operator and a base model. Adding a base model and a difference model results in the full [ADANN](#) architecture.

We now discuss some ideas in the scientific literature which are related to the [ADANN](#) methodology introduced in this paper. We roughly divide the related literature into three categories. First, we consider approaches similar to the idea of base models in the [ADANN](#) methodology, in the sense that classical numerical algorithms are somehow made trainable and are subsequently improved by means of [SGD](#)-type methods. One such approach – by which the [ADANN](#) methodology was partially inspired – is the *learning the random variable* methodology in [6] where *Monte Carlo neural networks* have been introduced which have the property that at suitable initializations the realizations of those networks correspond to sample realizations of Monte Carlo algorithms. Several approaches where Runge-Kutta methods for *ordinary differential equations* ([ODEs](#)) are improved by considering parts of the Butcher tableau as trainable parameters can, e.g., be found in [1, 16, 67, 73, 90]. Moreover, in [67] also certain parameters within numerical algorithms for [PDEs](#) are considered as trainable parameters. While the approaches in [1, 16, 67, 73, 90] are similar to the idea of base models in the [ADANN](#) methodology (and can be considered special cases of the [ADANN](#) methodology), they usually only train a handful of parameters which have an inherent meaning within the considered algorithms and in most cases even enforce some type of order conditions on the trained parameters, whereas we use a classical numerical algorithm as a starting point to design a base model but then do not restrict the model to stay within a class of known algorithms. In [30, 50] the restriction and prolongation operators in multigrid methods are considered as trainable parameters. In [93] [ANNs](#) are designed to emulate Runge-Kutta methods, not to learn solution operators, but to learn the dynamics of unknown [ODEs](#) from observed trajectories. In [3] finite difference approximations of spatial derivative operators for solutions of spatio-temporal [PDEs](#) are improved by means of [SGD](#)-type methods and subsequently used to perform time-integrations of the considered [PDEs](#). Similarly, [53] improve finite difference approximations of spatial derivatives in spatio-temporal [PDEs](#) but instead of directly improving the finite difference coefficients like in [3] they learn the truncation error by means of [ANNs](#).

Second, we mention approaches which are similar to the idea of difference models in the [ADANN](#) methodology, in the sense that [ANNs](#) are used to improve classical numerical algorithms by learning the difference between a classical algorithm and the corresponding target quantity. There are a number of approaches in the literature where [ANNs](#) are trained to approximate the difference between coarse-grid and fine-grid approximations of [PDE](#) solutions, notably within the context of large eddy simulations for the simulation of turbulent flows, c.f., e.g., [21, 28, 44, 52, 61, 65, 81, 86] and the references therein. There are also approaches where [ANNs](#) are used to learn the time stepping error of [ODE](#) integration schemes, c.f., e.g., [45, 84].

Third, we list some approaches which aim to combine classical methods with deep learning techniques but are neither close to the idea of base models nor to the idea of difference models in the [ADANN](#) methodology. A number of approaches use [ANNs](#) to guide classical methods by training the [ANNs](#) to identify regions where the classical methods need to be adjusted, c.f., e.g., [9, 19, 27, 79]. In [43] traditional iterative solvers are improved by adding some learnable parameters to the iterator. In [89] a convolutional neural network is used to efficiently approximate a linear projection which is then used as a component in a standard solver for fluid flows. In [11] [ANNs](#) are used to approximate optimal test spaces in the context of finite element methods.

Next we mention several other promising deep operator learning approaches in the literature, all of which can, in principle, be used as difference models within the [ADANN](#) methodology. One of the most successful methods in practice are the [FNOs](#) introduced in [60]. The derivation of [FNOs](#) is based on [59], an earlier paper by the same authors, where so-called graph kernel networks are employed. In [58] [FNOs](#) are generalized to more complicated geometries. In [10] the [FNO](#) methodology is extended by using Clifford layers, where calculations are performed in higher-dimensional non-commutative Clifford algebras. Another successful approach is the *deep operator network* ([DeepONet](#)) architecture introduced in [63], which consists of two types of [ANNs](#) that take as input the output space points and the input function values, respectively. For a comparison between the [DeepONet](#) and [FNO](#) methodologies we refer to [64]. In [56] [DeepONets](#) are generalized to a more sophisticated nonlinear architecture. In [75] operators on

Wasserstein spaces, for example, mean-field interactions of measures, are learned using networks based on standard ANNs and DeepONets. In [68] operators between Banach spaces are approximated by using random feature maps associated to operator-valued kernels. In [62] the entire flow map associated to ODEs is approximated by training a different ANN in each time-step and combining these ANNs with classical Runge-Kutta methods on different time scales. For approaches to build operator learning architectures based on convolutional neural networks, we refer, e.g., to [32, 38, 51, 78, 95]. We also refer to [14, 54] for estimates for approximation and generalization errors in network-based operator learning for PDEs. Finally, we refer to [10, Appendix D] and [47, Section 1.7.4] for more detailed literature overviews on operator learning approaches.

The remainder of this article is organized as follows. In Section 2 we introduce the main ideas of the ADANN methodology in an abstract setting. In Section 3 we describe in detail a specific base model design in the case of semilinear heat PDEs. In Section 4 we present four numerical simulations comparing the ADANN methodology to classical methods and operator learning methods from the literature.

2 Overview of the ADANN methodology

In this section we describe the ADANN methodology in an abstract setting. For this, we consider the problem of numerically approximating a measurable operator

$$\mathcal{S}: \mathcal{I} \rightarrow \mathcal{O} \quad (1)$$

where \mathcal{I} and \mathcal{O} are topological vector spaces¹. We assume that we are given a random input variable $\mathcal{J}: \Omega \rightarrow \mathcal{I}$ on a probability space $(\Omega, \mathcal{F}, \mathbb{P})$ and a continuous seminorm $\|\cdot\|: \mathcal{O} \rightarrow [0, \infty)$ on the output space. We measure the quality of a measurable approximation $\tilde{\mathcal{S}}: \mathcal{I} \rightarrow \mathcal{O}$ of the operator in (1) by means of the L^2 -error $\mathfrak{E}(\tilde{\mathcal{S}}) \in [0, \infty]$ given by

$$\mathfrak{E}(\tilde{\mathcal{S}}) = (\mathbb{E}[\|\tilde{\mathcal{S}}(\mathcal{J}) - \mathcal{S}(\mathcal{J})\|^2])^{1/2}. \quad (2)$$

Roughly speaking, the ADANN methodology proposed in this paper relies on the following three main ingredients to produce an efficient approximation of the operator \mathcal{S} :

- (i) *Base model with highly specialized initializations*: Based on a family of classical numerical approximation algorithms we design a tailor-made problem-specific ANN-type model together with a family of highly specialized initializations for the model and train the model to approximate \mathcal{S} (cf. Section 2.1).
- (ii) *Difference model*: We employ an existing operator learning model from the literature to approximate the difference between realizations of the base model of step (i) and the operator \mathcal{S} . Adding the difference model to the base model results in the *full ADANN model* (cf. Section 2.2).
- (iii) *Optimization over base model initializations*: We repeat the training of the full ADANN model with different (possibly random) highly specialized initializations of the base model and different standard random initializations of the difference model. The highly specialized initializations of the base model are chosen based on a suitable additional optimization approach aiming to minimize the error of the best full ADANN model over all training runs (cf. Section 2.3).

The combination of the above three components into the ADANN methodology is detailed in Section 2.4 in the form of pseudocodes.

2.1 Base model with highly specialized initializations

Constructing a base model requires a parametric family $\Phi_p: \mathcal{I} \rightarrow \mathcal{O}$, $p \in \mathfrak{P}$, of classical numerical algorithms² indexed over a parameter set \mathfrak{P} which approximate the operator \mathcal{S} in the sense that for every $p \in \mathfrak{P}$ we have that

$$\Phi_p \approx \mathcal{S}. \quad (3)$$

¹For example, we think of the mapping which assigns to all suitable initial values of a PDE of evolutionary type, the corresponding terminal value of the PDE.

²For example, we think of a family of Runge-Kutta and/or finite element methods.

A *base model* corresponding to the *designing algorithms* in (3) with $\mathbf{d}_{\text{Base}} \in \mathbb{N} = \{1, 2, 3, \dots\}$ trainable parameters is then given by a model $\mathcal{B} = (\mathcal{B}_W(g))_{(W,g) \in \mathbb{R}^{\mathbf{d}_{\text{Base}}} \times \mathcal{I}}: \mathbb{R}^{\mathbf{d}_{\text{Base}}} \times \mathcal{I} \rightarrow \mathcal{O}$ which can reproduce all the algorithms in (3). In mathematical terms, we require that for every $p \in \mathfrak{P}$ there exist model parameters $\mathbf{W}_p \in \mathbb{R}^{\mathbf{d}_{\text{Base}}}$ with

$$\mathcal{B}_{\mathbf{W}_p} = \Phi_p \approx \mathcal{S}. \quad (4)$$

Note that (4) implies that we already have parameters for the base model which yield reasonable approximations of \mathcal{S} . In the training of the base model we suggest to improve these approximations. Specifically, we propose to minimize the loss $\mathbf{L}^{(\text{Base})}: \mathbb{R}^{\mathbf{d}_{\text{Base}}} \rightarrow [0, \infty]$ satisfying³ for all $W \in \mathbb{R}^{\mathbf{d}_{\text{Base}}}$ that

$$\mathbf{L}^{(\text{Base})}(W) = \mathbb{E}[\|\mathcal{B}_W(\mathcal{J}) - \mathcal{S}(\mathcal{J})\|^2] = \mathfrak{E}(\mathcal{B}_W)^2 \quad (5)$$

by means of SGD-type processes initialized with model parameters from the set $\{\mathbf{W}_p: p \in \mathfrak{P}\}$.

For concrete examples of base models we refer to Section 3 where we derive designing algorithms and corresponding base models in the context of semilinear heat PDEs and to Sections 4.2.1, 4.3.1, and 4.4.1 where we specify the base models used in our numerical simulations.

2.2 Difference models

To combine a base model from Section 2.1 with deep operator learning models from the literature we propose to employ an existing deep operator learning model to approximate the difference between the operator \mathcal{S} and the base model. For this, we introduce a *difference model* $\mathcal{D} = (\mathcal{D}_\theta(g))_{(\theta,g) \in \mathbb{R}^{\mathbf{d}_{\text{Diff}}} \times \mathcal{I}}: \mathbb{R}^{\mathbf{d}_{\text{Diff}}} \times \mathcal{I} \rightarrow \mathcal{O}$ with $\mathbf{d}_{\text{Diff}} \in \mathbb{N}$ trainable parameters. For any base model parameters $\mathfrak{W} \in \mathbb{R}^{\mathbf{d}_{\text{Base}}}$ with $\mathfrak{E}(\mathcal{B}_{\mathfrak{W}}) \in (0, \infty)$ we then suggest to train the difference model by minimizing the loss $\mathbf{L}_{\mathfrak{W}}^{(\text{Diff})}: \mathbb{R}^{\mathbf{d}_{\text{Diff}}} \rightarrow [0, \infty]$ given⁴ for all $\theta \in \mathbb{R}^{\mathbf{d}_{\text{Diff}}}$ by

$$\mathbf{L}_{\mathfrak{W}}^{(\text{Diff})}(\theta) = \mathbb{E}[\|\mathcal{D}_\theta(\mathcal{J}) - (\mathfrak{E}(\mathcal{B}_{\mathfrak{W}}))^{-1}(\mathcal{S}(\mathcal{J}) - \mathcal{B}_{\mathfrak{W}}(\mathcal{J}))\|^2] \quad (6)$$

by means of SGD-type processes initialized in a standard random manner. Note that (6) suggests that, roughly speaking, we train the difference model to approximate a scaled difference between the operator \mathcal{S} and the base model $\mathcal{B}_{\mathfrak{W}}$ instead of the difference itself. This is done so that the training samples for the difference model are roughly of the same scale irrespective of the approximation quality of the base model.

Combining the base model of Section 2.1 and the difference model of this subsection, we define the *full ADANN model* $\mathcal{A} = (\mathcal{A}_{(W,\theta,\epsilon)}(g))_{(W,\theta,\epsilon,g) \in \mathbb{R}^{\mathbf{d}_{\text{Base}}} \times \mathbb{R}^{\mathbf{d}_{\text{Diff}}} \times \mathbb{R} \times \mathcal{I}}: \mathbb{R}^{\mathbf{d}_{\text{Base}}} \times \mathbb{R}^{\mathbf{d}_{\text{Diff}}} \times \mathbb{R} \times \mathcal{I} \rightarrow \mathcal{O}$ by imposing for all $W \in \mathbb{R}^{\mathbf{d}_{\text{Base}}}$, $\theta \in \mathbb{R}^{\mathbf{d}_{\text{Diff}}}$, $\epsilon \in \mathbb{R}$, $g \in \mathcal{I}$ that

$$\mathcal{A}_{(W,\theta,\epsilon)}(g) = \mathcal{B}_W(g) + \epsilon \mathcal{D}_\theta(g). \quad (7)$$

Observe that the scaling of the base model error in (6) implies that for every $\mathfrak{W} \in \mathbb{R}^{\mathbf{d}_{\text{Base}}}$, $\theta \in \mathbb{R}^{\mathbf{d}_{\text{Diff}}}$ with $\mathfrak{E}(\mathcal{B}_{\mathfrak{W}}) \in (0, \infty)$ the L^2 -error of the full ADANN model $\mathcal{A}_{(W,\theta,\epsilon(\mathcal{B}_{\mathfrak{W}}))}$ can be written as the product of the base and difference loss in the sense that

$$\begin{aligned} [\mathfrak{E}(\mathcal{A}_{(W,\theta,\epsilon(\mathcal{B}_{\mathfrak{W}}))})]^2 &= \mathbb{E}[\|\mathcal{B}_W(g) + \mathfrak{E}(\mathcal{B}_{\mathfrak{W}})\mathcal{D}_\theta(g) - \mathcal{S}(\mathcal{J})\|^2] \\ &= [\mathfrak{E}(\mathcal{B}_{\mathfrak{W}})]^2 \mathbb{E}[\|\mathcal{D}_\theta(g) + (\mathfrak{E}(\mathcal{B}_{\mathfrak{W}}))^{-1}(\mathcal{B}_W(g) - \mathcal{S}(\mathcal{J}))\|^2] \\ &= [\mathbf{L}^{(\text{Base})}(\mathfrak{W})][\mathbf{L}_{\mathfrak{W}}^{(\text{Diff})}(\theta)]. \end{aligned} \quad (8)$$

³In applications, the target operator \mathcal{S} is typically not known and has to be approximated for the training process. Such approximations can, for example, be obtained by using the same class of algorithms as the designing algorithms in (3) but with much finer discretizations.

⁴We note that, in applications, the base model error $\mathfrak{E}(\mathcal{B}_{\mathfrak{W}}) = (\mathbb{E}[\|\mathcal{B}_{\mathfrak{W}}(\mathcal{J}) - \mathcal{S}(\mathcal{J})\|^2])^{1/2}$ has to be approximated by a suitable Monte Carlo method (cf. line 9 in Algorithm 1).

2.3 Optimization over base model initializations

The results of SGD-type methods can strongly depend on their initializations and (4) suggests many choices of good initializations for the training of the base model. In view of this, we propose to repeat the training of the full ADANN model $R \in \mathbb{N}$ times where in each training run the base model is initialized with different parameters out of the set $\{\mathbf{W}_p: p \in \mathfrak{P}\}$ and the difference model is initialized in a standard random manner. The best trained full ADANN model over all training runs is then selected as the final approximation of the operator \mathcal{S} .

We aim to choose a sequence of initializations of the base model which minimizes the error of the best full ADANN model across all training runs. Very roughly speaking, this can be considered to be a black box optimization (also called derivative free optimization) problem with noise (cf., e.g., [15]) over the set of parameters \mathfrak{P} with the objective function given for all $p \in \mathfrak{P}$ by the (random) error of a trained full ADANN model whose base model has been initialized with \mathbf{W}_p and whose difference model has been initialized in a standard random manner. We abstractly model a black box optimization method for this optimization problem by a map

$$\mathfrak{o}: \left(\bigcup_{r=0}^{R-1} (\mathfrak{P} \times \mathbb{R})^r \right) \times \Omega \rightarrow \mathfrak{P}. \quad (9)$$

Intuitively speaking, for every $r \in \{0, 1, \dots, R-1\}$, $(p_1, e_1), \dots, (p_r, e_r) \in \mathfrak{P} \times [0, \infty)$ we think of $\mathbf{W}_{\mathfrak{o}((p_1, e_1), \dots, (p_r, e_r))}$ as the initialization for the training of the base model in the $(k+1)$ -th training run chosen by the black box optimization method \mathfrak{o} given that $(p_1, e_1), \dots, (p_k, e_k)$ are the initialization parameters and the corresponding errors of the trained full ADANN model of the first k training runs.

For more concrete specifications of the black box optimization method \mathfrak{o} we refer to Section 4.1 where we assume \mathfrak{o} to be a grid-based black box optimization method (cf. Section 4.1.1) and a heuristic exploration-exploitation black box optimization method (cf. Section 4.1.2). These two black box optimization approaches are the ones used in our numerical simulations in Section 4.

2.4 Pseudocode description of the ADANN methodology

In this section we describe in Algorithm 1 the ADANN methodology in the form of a pseudocode. Moreover, we also introduce a version of the ADANN methodology in Algorithm 2 which only relies on the base model of Section 2.1 and the optimization approach of Section 2.3 and does not include the difference model of Section 2.2.

In addition to the mathematical setting developed so far in Section 2, we consider the element-wise base loss $L_{\text{Base}}: \mathbb{R}^{\mathbf{d}_{\text{Base}}} \times \mathcal{I} \rightarrow [0, \infty)$ given for all $W \in \mathbb{R}^{\mathbf{d}_{\text{Base}}}$, $g \in \mathcal{I}$ by

$$L_{\text{Base}}(W, g) = \|\mathcal{B}_W(g) - \mathcal{S}(g)\|^2 \quad (10)$$

and the element-wise difference loss $L_{\text{Diff}}: \mathbb{R}^{\mathbf{d}_{\text{Base}}} \times \mathbb{R}^{\mathbf{d}_{\text{Diff}}} \times (0, \infty) \times \mathcal{I} \rightarrow [0, \infty)$ given for all $W \in \mathbb{R}^{\mathbf{d}_{\text{Base}}}$, $\theta \in \mathbb{R}^{\mathbf{d}_{\text{Diff}}}$, $\epsilon \in (0, \infty)$, $g \in \mathcal{I}$ by

$$L_{\text{Diff}}(W, \theta, \epsilon, g) = \|\mathcal{D}_\theta(g) - \left(\frac{1}{\epsilon}(\mathcal{S}(g) - \mathcal{B}_W(g))\right)\|^2. \quad (11)$$

Furthermore, we assume that for all $W \in \mathbb{R}^{\mathbf{d}_{\text{Base}}}$, $\epsilon \in (0, \infty)$, $g \in \mathcal{I}$ the functions $L_{\text{Base}}(\cdot, g): \mathbb{R}^{\mathbf{d}_{\text{Base}}} \rightarrow [0, \infty)$ and $L_{\text{Diff}}(W, \cdot, \epsilon, g): \mathbb{R}^{\mathbf{d}_{\text{Diff}}} \rightarrow [0, \infty)$ are differentiable. With these new objects we are now in a position to formulate the ADANN methodology in Algorithm 1 below.

Algorithm 1: ADANN methodology	
Setting: All mathematical objects introduced in Section 2 above	
Input: $V \in \mathbb{N}$ (Number of validation samples), $\gamma_{\text{Base}}, \gamma_{\text{Diff}} \in (0, \infty)$ (learning rates), $B_{\text{Base}}, B_{\text{Diff}} \in \mathbb{N}$ (batch sizes), $N_{\text{Base}}, N_{\text{Diff}} \in \mathbb{N}$ (number of train steps)	
Output: Approximation of \mathcal{S}	
1: $\mathfrak{J}_1^{(\text{validate})}, \dots, \mathfrak{J}_V^{(\text{validate})} \leftarrow$ generate i.i.d. realizations of \mathfrak{J}	# Get validation samples
2: for $r = 1, \dots, R$ do	
3: $\mathbf{p}_r \leftarrow \mathfrak{o}((\mathbf{p}_1, \epsilon_1), \dots, (\mathbf{p}_{r-1}, \epsilon_{r-1}))$	# Choose initialization parameters

```

4:  $\mathcal{W}_r \leftarrow \mathbf{W}_{\mathbf{p}_r}$  # Initialize base model
5: for  $n = 1, \dots, N_{\text{Base}}$  do
6:    $\mathcal{J}_1^{(\text{Base})}, \dots, \mathcal{J}_{B_{\text{Base}}}^{(\text{Base})} \leftarrow$  generate i.i.d. realizations of  $\mathcal{J}$  # Get train samples
7:    $\mathcal{W}_r \leftarrow \mathcal{W}_r - \frac{\gamma_{\text{Base}}}{B_{\text{Base}}} [\sum_{b=1}^{B_{\text{Base}}} (\nabla_{\mathcal{W}} L_{\text{Base}})(\mathcal{W}_r, \mathcal{J}_b^{(\text{Base})})]$  # Base model train step
8: end for
9:  $\epsilon_r \leftarrow (\frac{1}{V} [\sum_{v=1}^V \|\mathcal{B}_{\mathcal{W}_r}(\mathcal{J}_v^{(\text{validate})}) - \mathcal{S}(\mathcal{J}_v^{(\text{validate})})\|^2])^{1/2}$  # Base model validation error
10:  $\Theta_r \leftarrow$  standard random initialization # Initialize difference model
11: for  $n = 1, \dots, N_{\text{Diff}}$  do
12:    $\mathcal{J}_1^{(\text{Diff})}, \dots, \mathcal{J}_{B_{\text{Diff}}}^{(\text{Diff})} \leftarrow$  generate i.i.d. realizations of  $\mathcal{J}$  # Get train samples
13:    $\Theta_r \leftarrow \Theta_r - \frac{\gamma_{\text{Diff}}}{B_{\text{Diff}}} [\sum_{b=1}^{B_{\text{Diff}}} (\nabla_{\Theta} L_{\text{Diff}})(\mathcal{W}_r, \Theta_r, \epsilon_r, \mathcal{J}_b^{(\text{Diff})})]$  # Difference model train step
14: end for
15:  $\epsilon_r \leftarrow (\frac{1}{V} [\sum_{v=1}^V \|\mathcal{A}_{(\mathcal{W}_r, \Theta_r, \epsilon_r)}(\mathcal{J}_v^{(\text{validate})}) - \mathcal{S}(\mathcal{J}_v^{(\text{validate})})\|^2])^{1/2}$  # Full ADANN model validation error
16: end for
17:  $r^* \leftarrow \operatorname{argmin}_{r \in \{1, 2, \dots, R\}} \epsilon_r$  # Select full ADANN model with lowest validation error
18: return  $\mathcal{A}_{(\mathcal{W}^{(r^*)}, \Theta^{(r^*)}, \epsilon^{(r^*)})}$ 

```

Intuitively speaking, in some situations, adding a difference model to a base model might only introduce additional complexity without improving the approximation quality. For this reason we also introduce a version of the ADANN methodology without difference model in Algorithm 2 below. This version of the ADANN methodology only relies on the base model of Section 2.1 and the optimization approach of Section 2.3.

Algorithm 2: ADANN methodology without difference model

Setting: All mathematical objects introduced in Section 2 above

Input: $V \in \mathbb{N}$ (Number of validation samples), $\gamma_{\text{Base}} \in (0, \infty)$ (learning rate), $B_{\text{Base}} \in \mathbb{N}$ (batch size), $N_{\text{Base}} \in \mathbb{N}$ (number of train steps)

Output: Approximation of \mathcal{S}

```

1:  $\mathcal{J}_1^{(\text{validate})}, \dots, \mathcal{J}_V^{(\text{validate})} \leftarrow$  generate i.i.d. realizations of  $\mathcal{J}$  # Get validation samples
2: for  $r = 1, \dots, R$  do
3:    $\mathbf{p}_r \leftarrow \mathbf{o}((\mathbf{p}_1, \epsilon_1), \dots, (\mathbf{p}_{r-1}, \epsilon_{r-1}))$  # Choose initialization parameters
4:    $\mathcal{W}_r \leftarrow \mathbf{W}_{\mathbf{p}_r}$  # Initialize base model
5:   for  $n = 1, \dots, N_{\text{Base}}$  do
6:      $\mathcal{J}_1^{(\text{Base})}, \dots, \mathcal{J}_{B_{\text{Base}}}^{(\text{Base})} \leftarrow$  generate i.i.d. realizations of  $\mathcal{J}$  # Get train samples
7:      $\mathcal{W}_r \leftarrow \mathcal{W}_r - \frac{\gamma_{\text{Base}}}{B_{\text{Base}}} [\sum_{b=1}^{B_{\text{Base}}} (\nabla_{\mathcal{W}} L_{\text{Base}})(\mathcal{W}_r, \mathcal{J}_b^{(\text{Base})})]$  # Base model train step
8:   end for
9:    $\epsilon_r \leftarrow (\frac{1}{V} [\sum_{v=1}^V \|\mathcal{B}_{\mathcal{W}_r}(\mathcal{J}_v^{(\text{validate})}) - \mathcal{S}(\mathcal{J}_v^{(\text{validate})})\|^2])^{1/2}$  # Base model validation error
10: end for
11:  $r^* \leftarrow \operatorname{argmin}_{r \in \{1, 2, \dots, R\}} \epsilon_r$  # Select base model with lowest validation error
12: return  $\mathcal{B}_{\mathcal{W}^{(r^*)}}$ 

```

In the procedures described in Algorithms 1 and 2 above we made two major simplifications when compared to the methodology used in our numerical simulations in Section 4. First, in our numerical simulations we train the models with the ADAM optimizer with adaptive learning rates (see Appendix A for more details on the training process in our numerical simulations). However, for simplicity in Algorithms 1 and 2 we only described the case of the plain-vanilla SGD method with constant learning rates. Second, in all our numerical simulations the operator \mathcal{S} is not exactly known. Therefore, in our numerical simulations, we replace the exact operator \mathcal{S} with approximations of it in the base loss (cf. (10) above), in the difference loss (cf. (11) above), and in the validation errors (cf. lines 9 and 15 in Algorithm 1 and line 9 in Algorithm 2 above). These approximations are computed ahead of the training process for all train and validation samples. We note that, consequently, in our numerical simulations, the generation of training samples in lines 6 and 12 in Algorithm 1 and line 6 in Algorithm 2 is done by drawing samples from a fixed training set.

3 Derivation of a base model for semilinear heat PDEs

In this section we describe one way to design and initialize base models for the problem of approximating an operator mapping initial values to terminal values of a semilinear heat PDE (cf. Section 3.1). Specifically, we derive a family of approximation algorithms for the considered operator (cf. Section 3.2) and construct an ANN-type model together with a family of initializations for the model such that, at these initializations, the model emulates the approximation algorithms (cf. Section 3.3). We will use very similar base models and initializations to apply the ADANN methodology to a one-dimensional Sine-Gordon-type equation in our numerical simulations in Section 4.2.2.

3.1 One-dimensional semilinear heat PDEs

We now introduce the setting for the approximation problem considered in this section. For this, assume the mathematical setting developed in Section 2, let $T \in (0, \infty)$, let $f: \mathbb{R} \rightarrow \mathbb{R}$ be globally Lipschitz continuous, and for every $g \in C_{\text{per}}^2((0, 1), \mathbb{R})$ let $u_g: [0, T] \rightarrow C_{\text{per}}^2((0, 1), \mathbb{R})$ be a mild solution (cf., e.g., [13, 26, 74, 83]) of the PDE

$$\left(\frac{\partial}{\partial t} u_g\right)(t, x) = (\Delta_x u_g)(t, x) + f(u_g(t, x)), \quad (t, x) \in [0, T] \times (0, 1), \quad u_g(0) = g \quad (12)$$

with periodic boundary conditions, assume $\mathcal{I} = \mathcal{O} = C_{\text{per}}^2((0, 1), \mathbb{R})$, and assume that the operator $\mathcal{S}: \mathcal{I} \rightarrow \mathcal{O}$ we want to approximate is given for all $g \in \mathcal{I}$ by

$$\mathcal{S}(g) = u_g(T). \quad (13)$$

3.2 Designing algorithms for the base model

We now derive a family of approximation algorithms for the operator \mathcal{S} in (13) which will serve as designing algorithms for the base model derived in this section. Roughly speaking, the algorithms are based on discretizing the space domain of the PDE in (12) with the finite difference method and on discretizing the time domain of the PDE in (12) with a family of second order *linearly implicit Runge-Kutta* (LIRK) methods.

3.2.1 Spatial finite difference discretization

For the spatial discretization of the PDE in (12) consider $N \in \mathbb{N}$ grid points $\mathfrak{r}_1, \mathfrak{r}_2, \dots, \mathfrak{r}_N \in [0, 1]$ given for all $i \in \{1, 2, \dots, N\}$ by $\mathfrak{r}_i = \frac{i-1}{N}$, let $\mathbf{e}: \mathcal{I} \rightarrow \mathbb{R}^N$ be the evaluation on the grid points given for all $g \in \mathcal{I}$ by

$$\mathbf{e}(g) = (g(\mathfrak{r}_1), g(\mathfrak{r}_2), \dots, g(\mathfrak{r}_N)), \quad (14)$$

and consider the corresponding finite difference discretization of the Laplace operator on $(0, 1)$ with periodic boundary conditions given by

$$A = N^2 \begin{pmatrix} -2 & 1 & 0 & 0 & \cdots & 0 & 0 & 1 \\ 1 & -2 & 1 & 0 & \cdots & 0 & 0 & 0 \\ 0 & 1 & -2 & 1 & \cdots & 0 & 0 & 0 \\ & & & & \ddots & & & \\ 0 & 0 & 0 & 0 & \cdots & 1 & -2 & 1 \\ 1 & 0 & 0 & 0 & \cdots & 0 & 1 & -2 \end{pmatrix} \in \mathbb{R}^{N \times N}. \quad (15)$$

Under suitable assumptions, we expect for all $g \in \mathcal{I}$ that

$$A(\mathbf{e}(g)) \approx \mathbf{e}(\Delta g). \quad (16)$$

Using this spatial discretization on the PDE in (12) results in an initial value ODE. Formally, for every $g \in \mathbb{R}^N$ let $\mathbf{u}_g \in C^1([0, T], \mathbb{R}^N)$ satisfy⁵ for all $t \in [0, T]$ that

$$\left(\frac{\partial}{\partial t} \mathbf{u}_g\right)(t) = A\mathbf{u}_g(t) + f(\mathbf{u}_g(t)) \quad \text{and} \quad \mathbf{u}_g(0) = \mathbf{g}. \quad (17)$$

⁵Throughout this paper for every $h: \mathbb{R} \rightarrow \mathbb{R}$, $n \in \mathbb{N}$, $x = (x_1, x_2, \dots, x_n) \in \mathbb{R}^n$ we denote by $h(x) \in \mathbb{R}^n$ the vector given by $h(x) = (h(x_1), h(x_2), \dots, h(x_n))$.

Under suitable assumptions we expect for all $g \in \mathcal{I}$ that

$$\mathbf{u}_{\mathbf{e}(g)}(T) \approx \mathbf{e}(u_g(T, \cdot)) = \mathbf{e}(\mathcal{S}(g)). \quad (18)$$

3.2.2 Temporal linearly implicit Runge-Kutta (LIRK) discretizations

In the next step we use a parametric family of second order LIRK methods to discretize the ODE in (17). We only introduce the family of LIRK methods here and refer to Appendix B for a more detailed derivation.

Specifically, let $M \in \mathbb{N}$ be the numbers of time steps, let $H = T/M$ be the corresponding time step size, let $I \in \mathbb{R}^{N \times N}$ be the identity matrix, assume $\mathfrak{P} \subseteq (0, \infty)^2$, and for all parameters $p = (p_1, p_2) \in \mathfrak{P}$ let the LIRK time step $\phi_p: \mathbb{R}^N \rightarrow \mathbb{R}^N$ satisfy for all $U, k_1, k_2 \in \mathbb{R}^N$ with

$$k_1 = (I - Hp_2A)^{-1}(AU + f(U)) \quad \text{and} \quad (19)$$

$$k_2 = (I - Hp_2A)^{-1}(A(U + H2p_1(\frac{1}{2} - p_2)k_1) + f(U + Hp_1k_1)) \quad (20)$$

that

$$\phi_p(U) = U + H \left[\left(1 - \frac{1}{2p_1}\right)k_1 + \left(\frac{1}{2p_1}\right)k_2 \right]. \quad (21)$$

For every choice of parameters $p \in \mathfrak{P}$ the corresponding LIRK algorithm $\psi_p: \mathbb{R}^N \rightarrow \mathbb{R}^N$ for the ODE in (17) is then given by

$$\psi_p = \underbrace{\phi_p \circ \dots \circ \phi_p}_{M\text{-times}}. \quad (22)$$

Under suitable assumptions (cf. (18) above) we then expect that for all $p \in \mathfrak{P}$, $g \in \mathcal{I}$ we have that

$$\psi_p(\mathbf{e}(g)) \approx \mathbf{u}_{\mathbf{e}(g)}(T) \approx \mathbf{e}(\mathcal{S}(g)). \quad (23)$$

Finally, let $\mathbf{i}: \mathbb{R}^N \rightarrow \mathcal{O}$ be an interpolation operator on the grid points in the sense that for all $\mathbf{g} = (\mathbf{g}_1, \mathbf{g}_2, \dots, \mathbf{g}_N) \in \mathbb{R}^N$, $i \in \{1, 2, \dots, N\}$ we have that

$$[\mathbf{i}(\mathbf{g})](\mathbf{r}_i) = \mathbf{g}_i \quad (24)$$

and assume that for every $p \in \mathfrak{P}$ the designing algorithm $\Phi_p: \mathcal{I} \rightarrow \mathcal{O}$ is given by

$$\Phi_p = \mathbf{i} \circ \psi_p \circ \mathbf{e}. \quad (25)$$

Combining (23), (24), and (25) we expect, under suitable assumptions, that for all $p \in \mathfrak{P}$, $g \in \mathcal{I}$ we have that

$$\Phi_p(g) = \mathbf{i}(\psi_p(\mathbf{e}(g))) \approx \mathbf{i}(\mathbf{e}(\mathcal{S}(g))) \approx \mathcal{S}. \quad (26)$$

For a more rigorous error analysis for the designing algorithms in (26) we refer, e.g., to [33, 48, 87, 88] and the references therein.

3.2.3 A compact reformulation of the designing algorithms

To make the designing algorithms of Section 3.2.2 amenable to be written as realizations of an ANN-type base model we now present a more compact reformulation of the LIRK time steps in (22). To this end for every $p = (p_1, p_2) \in \mathfrak{P}$ let $\mathbf{w}_p = (\mathbf{w}_{p,i})_{i \in \{1, 2, \dots, 5\}} \in (\mathbb{R}^{N \times N})^5$ satisfy

$$\mathbf{w}_{p,1} = (I - Hp_2A)^{-1}(I + H(1 - p_2)A) + H^2(\frac{1}{2} - p_2)[(I - Hp_2A)^{-1}A]^2, \quad (27)$$

$$\mathbf{w}_{p,2} = H(1 - \frac{1}{2p_1})(I - Hp_2A)^{-1} + H^2(\frac{1}{2} - p_2)(I - Hp_2A)^{-1}A(I - Hp_2A)^{-1}, \quad (28)$$

$$\mathbf{w}_{p,3} = H(\frac{1}{2p_1})(I - Hp_2A)^{-1}, \quad \mathbf{w}_{p,4} = (I - Hp_2A)^{-1}(I + H(p_1 - p_2)A), \quad (29)$$

$$\text{and} \quad \mathbf{w}_{p,5} = Hp_1(I - Hp_2A)^{-1}. \quad (30)$$

Note that (19), (20), (21), (27), (28), (29), and (30) imply that for all $p \in \mathfrak{P}$, $U \in \mathbb{R}^N$ we have that

$$\phi_p(U) = \mathbf{w}_{p,1}U + \mathbf{w}_{p,2}f(U) + \mathbf{w}_{p,3}f(\mathbf{w}_{p,4}U + \mathbf{w}_{p,5}f(U)). \quad (31)$$

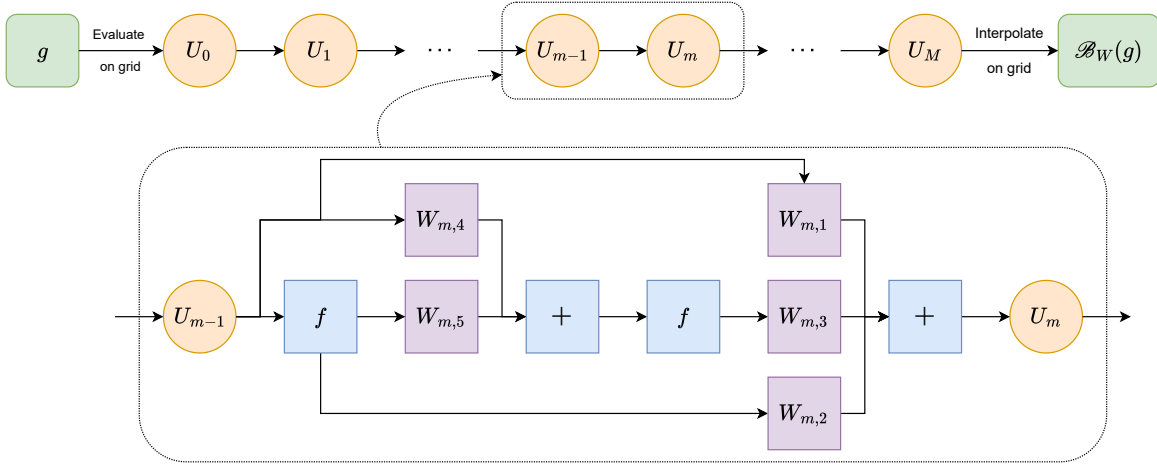


Figure 1: Graphical illustration for the base model defined in (32) and (33).

3.3 Designing the base model and its initializations

Roughly speaking, we propose to design the base model by considering the matrices in (31) as trainable parameters (see Figure 1 for an illustration of the base model) and to use (27)–(30) to define the initialization parameters. More precisely, assume that $\mathbf{d}_{\text{Base}} = 5N^{2d}M$, assume⁶ that the base model $\mathcal{B}: ((\mathbb{R}^{N \times N})^5)^M \times \mathcal{I} \rightarrow \mathcal{O}$ is given for all $W = ((W_{m,i})_{i \in \{1,2,\dots,5\}})_{m \in \{1,2,\dots,M\}} \in ((\mathbb{R}^{N \times N})^5)^M$, $g \in \mathcal{I}$, $U_0, U_1, \dots, U_M \in \mathbb{R}^N$ with $U_0 = \mathbf{e}(g)$ and $\forall m \in \{1, 2, \dots, M\}$:

$$U_m = W_{m,1}U_{m-1} + W_{m,2}f(U_{m-1}) + W_{m,3}f(W_{m,4}U_{m-1} + W_{m,5}f(U_{m-1})) \quad (32)$$

by

$$\mathcal{B}_W(g) = \mathbf{i}(U_M), \quad (33)$$

and for every $p \in \mathfrak{P}$ assume that the initialization parameters $\mathbf{W}_p \in ((\mathbb{R}^{N \times N})^5)^M$ are given by

$$\mathbf{W}_p = \underbrace{(\mathbf{w}_p, \dots, \mathbf{w}_p)}_{M\text{-times}}. \quad (34)$$

Note that (22), (25), (31), (32), and (33) demonstrate that for all $p \in \mathfrak{P}$ it holds that

$$\mathcal{B}_{\mathbf{W}_p} = \left(\mathbf{i} \circ \underbrace{(\phi_p \circ \dots \circ \phi_p)}_{M\text{-times}} \circ \mathbf{e} \right) = \left(\mathbf{i} \circ \psi_p \circ \mathbf{e} \right) = \Phi_p. \quad (35)$$

Roughly speaking, we thus have constructed a base model which is able to reproduce all the designing algorithms we derived in Section 3.2. Combining this with (26) implies that, under suitable assumptions, we have for all $p \in \mathfrak{P}$ that

$$\mathcal{B}_{\mathbf{W}_p} \approx \mathcal{S}. \quad (36)$$

4 Numerical simulations

In this section we numerically test the ADANN methodology as described in Section 2 in the case of four operators related to parametric PDE problems and compare its performance with existing operator learning architectures and classical numerical methods. First, in Section 4.1 we describe the black box optimization methods used in the ADANN methodology in our numerical simulations. We then consider the numerical approximation of operators mapping initial values to terminal values of one and

⁶In order to structure the parameters of the base model, we slightly abuse the notation and identify $\mathbb{R}^{\mathbf{d}_{\text{Base}}} \simeq ((\mathbb{R}^{N^d \times N^d})^5)^M$.

two-dimensional Sine-Gordon-type equations in Section 4.2, the numerical approximation of an operator mapping initial values to terminal values of the viscous Burgers equation in Section 4.3, and the numerical approximation of an operator mapping source terms to terminal values of a reaction-diffusion equation in Section 4.4.

In every considered problem, all models (i.e., all base models, all difference models, and all other operator learning models) are trained using the same training and validation set with the Adam optimizer with adaptive learning rates (cf. Appendix A for a detailed description of our adaptive training procedure). Moreover, to provide a fair comparison between the ADANN methodology and other operator learning architectures we repeat the training of every operator learning model several times with different initializations and select the best performing trained model over all training runs as the approximation for that architecture. In every considered problem, the L^2 -errors of all methods are approximated using a Monte Carlo approximation based on the same test set. The parameters chosen to generate train, validation, and test sets, as well as additional hyperparameters for each problem are listed in Table 5 in Appendix A.

All the simulations were run on a remote machine on <https://vast.ai> equipped with an NVIDIA GEFORCE RTX 3090 GPU with 24 GB RAM and an XEON® E5-2698 v3 CPU with 32 GB of total system RAM. As the evaluation time of models on GPUs can be highly variable, we report the average evaluation time over 1000 test set evaluations for each method. The code for all numerical simulations is available at <https://github.com/vwurstep/ADANNs>.

4.1 Black box optimizers

One of the three main components of the ADANN methodology described in Section 2 is to repeat the training of the full ADANN model with different initializations and to use a black box optimization method over the highly specialized initializations of the base model to aim to minimize the error of the best trained full ADANN model over all training runs (cf. Section 2.3). In principle any black box optimization method can be employed for the optimization problem arising in the ADANN methodology and we tested several black box optimization methods from the scikit-optimize library (see [35]) such as Gaussian process optimization and decision tree based optimization, but they failed to give satisfactory results. Consequently, in our numerical simulations we restricted ourselves to two optimization approaches which we describe in detail in this section.

The first one is a simple grid-based black box optimization method. We describe this approach in Section 4.1.1. The second one is a heuristic black box optimization approach aiming to achieve an exploration-exploitation trade-off using an approximation of the objective function based on previously evaluated points. We describe this approach in Section 4.1.2.

4.1.1 Grid-based black box optimizer

In this section we discuss a grid-based black box optimization approach to minimize a considered objective function. Roughly speaking, a grid-based black box optimizer simply evaluates the objective function at all points on a grid irrespective of the outcome of previous evaluations. To describe this approach more formally, we will specify the black box optimizer \mathfrak{o} introduced in the description of the ADANN methodology in Section 2.3 to such a grid-based black box optimizer.

For this, assume the setting developed in Section 2, let $g_1, g_2, \dots, g_R \in \mathfrak{P}$, and assume that for all $r \in \{0, 1, \dots, R-1\}$, $(p_1, e_1), \dots, (p_r, e_r) \in \mathfrak{P} \times \mathbb{R}$ we have that

$$\mathfrak{o}((p_1, e_1), \dots, (p_r, e_r)) = g_{r+1}. \quad (37)$$

Roughly speaking, in this context we think of R as the number of grid points and we think of g_1, g_2, \dots, g_R as points on a grid in \mathfrak{P} .

4.1.2 Heuristic exploration-exploitation black box optimizer

In this section we discuss a heuristic exploration-exploitation black box optimization approach to minimize a considered objective function. Roughly speaking, the proposed black box optimization approach can be divided into two phases. In the first phase, the objective function is evaluated at several initial

points, which may be chosen randomly, in its domain. In the second phase, every new evaluation point is chosen by randomly sampling a point according to a probability density function which favors areas with lower approximate objective function values but penalizes areas which are close to previously evaluated points. The approximate objective function values in the second phase are obtained by a suitable regression or interpolation technique based on earlier evaluations of the objective function. To describe this approach more formally, we will specify the black box optimizer \mathfrak{o} introduced in the description of the [ADANN](#) methodology in Section 2.3 to such a heuristic exploration-exploitation black box optimizer.

For this assume the setting developed in Section 2, let $\mathbf{p} \in \mathbb{N}$, $c_1, c_2 \in (0, \infty)$, $Q \in \{0, 1, \dots, R\}$, assume that \mathfrak{P} is a compact subset of \mathbb{R}^p , let $\mathfrak{Q}_r: \Omega \rightarrow \mathfrak{P}$, $r \in \{1, 2, \dots, Q\}$, be random variables, let $\mathcal{r}: \left(\cup_{r=0}^{R-1} (\mathfrak{P} \times \mathbb{R})^r\right) \rightarrow C(\mathfrak{P}, (0, \infty))$, $\mathcal{t}: \left(\cup_{r=0}^{R-1} (\mathfrak{P} \times \mathbb{R})^r\right) \rightarrow C(\mathfrak{P}, (0, \infty))$, $\mathfrak{D}: \left(\cup_{r=0}^{R-1} (\mathfrak{P} \times \mathbb{R})^r\right) \rightarrow C(\mathfrak{P}, (0, \infty))$, and $\mathfrak{d}: \left(\cup_{r=0}^{R-1} (\mathfrak{P} \times \mathbb{R})^r\right) \rightarrow C(\mathfrak{P}, (0, \infty))$ satisfy for all $r \in \{0, 1, \dots, R-1\}$, $\mathbf{p} = ((p_1, e_1), \dots, (p_r, e_r)) \in (\mathfrak{P} \times \mathbb{R})^r$ that

$$\mathfrak{t}_{\mathbf{p}} = \mathcal{r}_{\mathbf{p}} + \sum_{k=1}^r \frac{c_1 \min(\mathcal{r}_{\mathbf{p}})}{c_1 + \|p_k - \cdot\|_{\mathbb{R}^p}}, \quad \mathfrak{D}_{\mathbf{p}} = \exp\left(-\frac{c_2(\mathfrak{t}_{\mathbf{p}} - \min(\mathcal{r}_{\mathbf{p}}))}{\min(\mathcal{r}_{\mathbf{p}})}\right), \quad \text{and} \quad \mathfrak{d}_{\mathbf{p}} = \frac{\mathfrak{D}_{\mathbf{p}}}{\int_{\mathfrak{P}} \mathfrak{D}_{\mathbf{p}}(q) dq}, \quad (38)$$

for every $\mathbf{p} \in \cup_{r=Q}^{R-1} (\mathfrak{P} \times \mathbb{R})^r$ let $\mathfrak{X}_{\mathbf{p}}: \Omega \rightarrow \mathfrak{P}$ be a random variable which satisfies for all $B \in \mathcal{B}(\mathfrak{P})$ that

$$\mathbb{P}(\mathfrak{X}_{\mathbf{p}} \in B) = \int_B \mathfrak{d}_{\mathbf{p}}(q) dq, \quad (39)$$

and assume for all $r \in \{0, 1, \dots, R-1\}$, $\mathbf{p} = ((p_1, e_1), \dots, (p_r, e_r)) \in (\mathfrak{P} \times \mathbb{R})^r$ that

$$\mathfrak{o}(\mathbf{p}) = \begin{cases} \mathfrak{Q}_{r+1}, & r < Q \\ \mathfrak{X}_{\mathbf{p}}, & r \geq Q. \end{cases} \quad (40)$$

Roughly speaking, we think of $\mathfrak{Q}_1, \dots, \mathfrak{Q}_Q$ as the initial points at which the objective function is evaluated and for every number $r \in \{Q+1, Q+2, \dots, R\}$ and every sequence $\mathbf{p} \in (\mathfrak{P} \times \mathbb{R})^r$ of previous evaluations

- (i) we think of $\mathfrak{X}_{\mathbf{p}}$ as the point at which the objective function is evaluated in the r -th step of the optimization process given that the previous evaluations are given by \mathbf{p} ,
- (ii) we think of $\mathfrak{d}_{\mathbf{p}}$ as the probability density function obtained from normalizing $\mathfrak{D}_{\mathbf{p}}$ which is used to sample the point $\mathfrak{X}_{\mathbf{p}}$,
- (iii) we think of $\mathfrak{D}_{\mathbf{p}}$ as an unnormalized probability density function which inverts the values of $\mathfrak{t}_{\mathbf{p}}$, that is, $\mathfrak{D}_{\mathbf{p}}$ assigns higher probabilities to areas where $\mathfrak{t}_{\mathbf{p}}$ has lower values and lower probabilities where $\mathfrak{t}_{\mathbf{p}}$ has higher values,
- (iv) we think of $\mathfrak{t}_{\mathbf{p}}$ as a penalized version of $\mathcal{r}_{\mathbf{p}}$ where the function values close to previous evaluation points in \mathbf{p} are increased, and
- (v) we think of $\mathcal{r}_{\mathbf{p}}$ as an approximation of the objective function based on the previous evaluations in \mathbf{p} .

In all our numerical simulations we choose the hyperparameters $c_1 = 0.005$ and $c_2 = 100$ and we take \mathcal{r} to be a smoothened RBF interpolation as implemented in [82].

4.2 Sine-Gordon-type equation

In this section we test the [ADANN](#) methodology without difference model as described in Section 2.4 (cf. Algorithm 2) in the case of operators mapping initial values to terminal values of one and two-dimensional Sine-Gordon-type equations. We introduce below the considered Sine-Gordon-type equations and the corresponding operators. The base models used for both the one and two-dimensional case are defined in Section 4.2.1 and the results of our numerical simulations are presented in Section 4.2.2 for the one-dimensional case and in Section 4.2.3 for the two-dimensional case.

Throughout Section 4.2 assume the mathematical setting developed in Section 2, let $d \in \{1, 2\}$, $T = 2$, $c = \frac{1}{100}$, for every $g \in H_{\text{per}}^2((0, 1)^d; \mathbb{R})$ let $u_g: [0, T] \rightarrow H_{\text{per}}^2((0, 1)^d; \mathbb{R})$ be a mild solution of the PDE

$$\left(\frac{\partial}{\partial t} u_g\right)(t, x) = c(\Delta_x u_g)(t, x) + \sin(u_g(t, x)), \quad (t, x) \in [0, T] \times (0, 1)^d, \quad u_g(0) = g \quad (41)$$

with peridodic boundary conditions, assume $\mathcal{I} = \mathcal{O} = H_{\text{per}}^2((0, 1)^d; \mathbb{R})$, and assume that the operator $\mathcal{S}: \mathcal{I} \rightarrow \mathcal{O}$ we want to approximate is given for all $g \in \mathcal{I}$ by

$$\mathcal{S}(g) = u_g(T). \quad (42)$$

Moreover, assume that the initial value $\mathcal{J}: \Omega \rightarrow \mathcal{I}$ is $\mathcal{N}(0, 10^{10}(10^{2.5} \text{id}_{\mathcal{I}} - \Delta_x)^{-4})$ -distributed where Δ_x is the Laplace operator on $L^2((0, 1)^d; \mathbb{R})$ with periodic boundary conditions, fix a space discretization $N \in \mathbb{N}$, and assume for all $h \in \mathcal{O}$ that

$$\|h\|^2 = \frac{1}{N^d} \left[\sum_{\mathbf{x} \in \{\frac{0}{N}, \frac{1}{N}, \dots, \frac{N-1}{N}\}^d} (h(\mathbf{x}))^2 \right] \approx \int_{(0,1)^d} (h(x))^2 dx. \quad (43)$$

We recall that our goal is to find an approximation $\tilde{\mathcal{S}}: \mathcal{I} \rightarrow \mathcal{O}$ of the operator in (42) which minimizes the L^2 -error $\mathfrak{E}(\tilde{\mathcal{S}}) \in [0, \infty]$ given by

$$\mathfrak{E}(\tilde{\mathcal{S}}) = (\mathbb{E}[\|\tilde{\mathcal{S}}(\mathcal{J}) - \mathcal{S}(\mathcal{J})\|^2])^{1/2} \approx \left(\mathbb{E} \left[\int_{(0,1)^d} (\tilde{\mathcal{S}}(\mathcal{J})(x) - u_{\mathcal{J}}(T, x))^2 dx \right] \right)^{1/2}. \quad (44)$$

4.2.1 Base model for the Sine-Gordon-type equation

We now describe the base model that we use in the ADANN methodology to approximate the operator in (42). Roughly speaking, we use the base model derived in Section 3 with the initialization parameters adjusted to the considered Sine-Gordon-type equations. A graphical illustration for this base model can be found in Figure 1.

Specifically, let $M \in \mathbb{N}$, let $\mathbf{e}: \mathcal{I} \rightarrow \mathbb{R}^{N^d}$ be an evaluation operator on the grid $\{\frac{0}{N}, \frac{1}{N}, \dots, \frac{N-1}{N}\}^d$ and let $\mathbf{i}: \mathbb{R}^{N^d} \rightarrow \mathcal{O}$ be a corresponding interpolation operator (cf. (14) and (24)), let $f = \sin$, and assume that $\mathbf{d}_{\text{Base}} = 5N^{2d}M$. We then assume⁷ that the base model $\mathcal{B}: ((\mathbb{R}^{N^d \times N^d})^5)^M \times \mathcal{I} \rightarrow \mathcal{O}$ is given for all $W = ((W_{m,i})_{i \in \{1, 2, \dots, 5\}})_{m \in \{1, 2, \dots, M\}} \in ((\mathbb{R}^{N^d \times N^d})^5)^M$, $g \in \mathcal{I}$, $U_0, U_1, \dots, U_M \in \mathbb{R}^{N^d}$ with $U_0 = \mathbf{e}(g)$ and $\forall m \in \{1, 2, \dots, M\}$:

$$U_m = W_{m,1}U_{m-1} + W_{m,2}f(U_{m-1}) + W_{m,3}f(W_{m,4}U_{m-1} + W_{m,5}f(U_{m-1})) \quad (45)$$

by

$$\mathcal{B}_W(g) = \mathbf{i}(U_M). \quad (46)$$

To define the family of initialization parameters $\mathbf{W}_p \in ((\mathbb{R}^{N^d \times N^d})^5)^M$, $p \in \mathfrak{P}$, for the base model let $H = T/M$, let $I \in \mathbb{R}^{N^d \times N^d}$ be the identity matrix, let $A \in \mathbb{R}^{N^d \times N^d}$ be the finite difference discretization of the Laplace operator on $(0, 1)^d$ with periodic boundary conditions, corresponding to the evaluation operator \mathbf{e} (cf. (15) for a definition of A in the case $d = 1$), assume $\mathfrak{P} = (0.1, 1.2) \times (0.25, 1.2)$, and for every $p = (p_1, p_2) \in \mathfrak{P}$ let $\mathbf{w}_p = (\mathbf{w}_{p,i})_{i \in \{1, 2, \dots, 5\}} \in (\mathbb{R}^{N^d \times N^d})^5$ satisfy

$$\mathbf{w}_{p,1} = (I - Hp_2cA)^{-1}(I + H(1 - p_2)cA) + H^2(\frac{1}{2} - p_2)[(I - Hp_2cA)^{-1}cA]^2, \quad (47)$$

$$\mathbf{w}_{p,2} = H(1 - \frac{1}{2p_1})(I - Hp_2cA)^{-1} + H^2(\frac{1}{2} - p_2)(I - Hp_2cA)^{-1}cA(I - Hp_2cA)^{-1}, \quad (48)$$

$$\mathbf{w}_{p,3} = H(\frac{1}{2p_1})(I - Hp_2cA)^{-1}, \quad \mathbf{w}_{p,4} = (I - Hp_2cA)^{-1}(I + H(p_1 - p_2)cA), \quad (49)$$

⁷In order to structure the parameters of the base model, we slightly abuse the notation and identify $\mathbb{R}^{\mathbf{d}_{\text{Base}}} \simeq ((\mathbb{R}^{N^d \times N^d})^5)^M$.

Method	Estimated L^2 -error in (44)	Average evaluation time for 2^{14} test samples over 1000 runs (in s)	Number of trainable parameters	Precomputation time (in s)
ANN (arch.: (64, 512, 512, 64))	0.092265	0.0008	328768	380
ANN (arch.: (64, 512, 2048, 512, 64))	0.059692	0.0036	2165824	389
ANN (arch.: (64, 512, 2048, 8192, 2048, 512, 64))	0.045492	0.0533	35730496	605
FNO (nr. modes: 8, width: 20, depth: 3)	0.033482	0.0216	24545	1042
FNO (nr. modes: 16, width: 30, depth: 4)	0.024216	0.0327	84935	1387
FNO (nr. modes: 32, width: 40, depth: 5)	0.021383	0.0455	301745	1700
FDM (2 Crank-Nicolson time steps)	0.246219	0.0008	0	0
FDM (4 Crank-Nicolson time steps)	0.057750	0.0016	0	0
FDM (8 Crank-Nicolson time steps)	0.017722	0.0032	0	0
ADANN base - grid (2 time steps)	0.023020	0.0009	40960	933
ADANN base - grid (4 time steps)	0.009251	0.0016	81920	1344
ADANN base - grid (8 time steps)	0.003733	0.0031	163840	2647
ADANN base - EE (2 time steps)	0.023950	0.0008	40960	451
ADANN base - EE (4 time steps)	0.009754	0.0016	81920	692
ADANN base - EE (8 time steps)	0.004596	0.0031	163840	1178

Table 1: Comparison of the performance of different methods for the approximation of the operator in (42) mapping initial values to terminal values of the Sine-Gordon-type equation in (41) in the case $d = 1$.

$$\text{and } \mathbf{w}_{p,5} = Hp_1(I - Hp_2cA)^{-1}. \quad (50)$$

We then assume that for every $p \in \mathfrak{P}$ the parameters $\mathbf{W}_p \in ((\mathbb{R}^{N^d \times N^d})^5)^M$ are given by

$$\mathbf{W}_p = \underbrace{(\mathbf{w}_p, \dots, \mathbf{w}_p)}_{M\text{-times}}. \quad (51)$$

Roughly speaking, for every $p \in \mathfrak{P}$ we have that

$$\mathcal{B}_{\mathbf{w}_p} \approx \mathcal{S} \quad (52)$$

corresponds to an approximation of the Sine-Gordon-type equation in (41) based on a finite difference discretization in space and a [LIRK](#) approximation in time where the parameters p corresponds to the parameters of the [LIRK](#) method (cf. Appendix B).

4.2.2 Numerical results for the one-dimensional Sine-Gordon-type equation

In this section we present numerical results for the approximation of the operator in (41) in the case $d = 1$. We test the [ADANN](#) methodology without difference model (cf. Algorithm 2) with the base model and the corresponding initializations defined in Section 4.2.1, parameter space $\mathfrak{P} = (0.1, 1.2) \times (0.25, 1.2)$, space discretization $N = 64$, number of time steps $M \in \{2, 4, 8\}$, and both a grid-based black box optimizer as described in Section 4.1.1 (see rows 10-12 in Table 1 and Figure 3) and our heuristic exploration-exploitation black box optimizer as described in Section 4.1.2 (see rows 13-15 in Table 1 and Figure 4). We also test different [ANN](#) models with *Gaussian Error Linear Unit* ([GELU](#)) activation function (see rows 1-3 in Table 1), [FNO](#) models (see rows 4-6 in Table 1), and classical methods (see rows 7-9 in Table 1) for comparison. As classical methods we use the untrained base model $\mathcal{B}_{\mathbf{w}_{(0.5,0.5)}}$ with $M \in \{2, 4, 8\}$ time steps, corresponding, roughly speaking, to a finite difference discretization in space and a Crank–Nicolson explicit midpoint [LIRK](#) discretization in time (cf. Appendix B.3). The performance of all considered methods is summarized in Table 1 and graphically illustrated in Figure 2. In addition, some of the approximations for a randomly chosen test sample are shown in Figure 5.

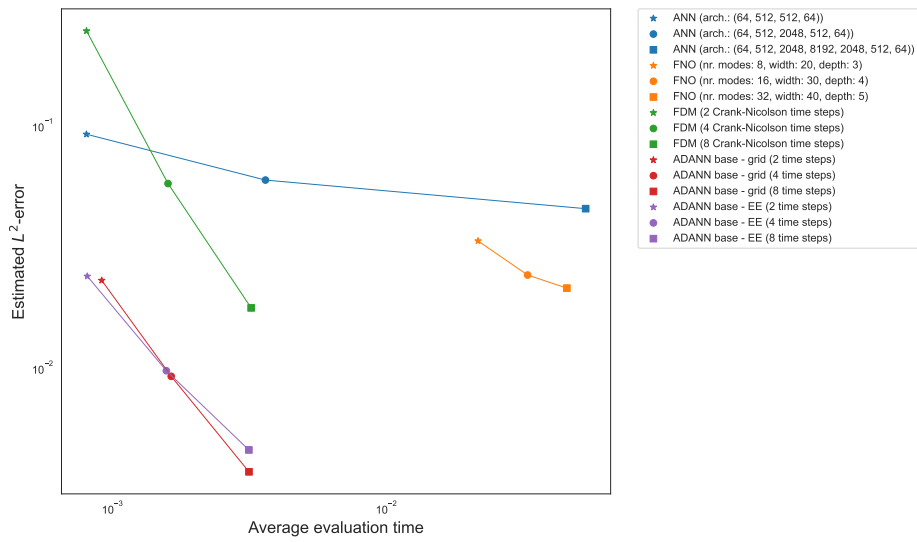


Figure 2: Graphical illustration of the performance of the methods in Table 1.

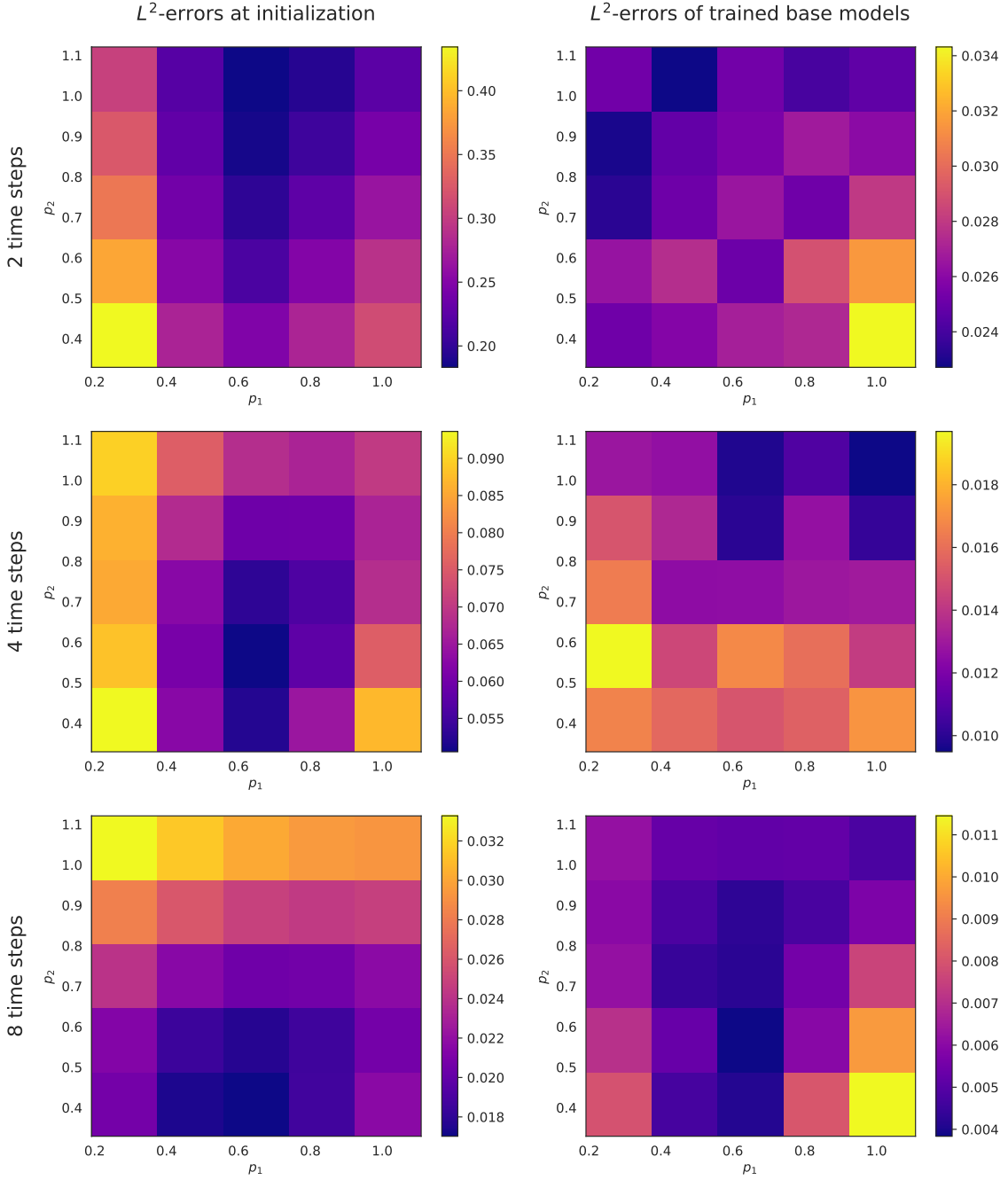


Figure 3: Illustration of the [ADANN](#) methodology without difference model (cf. Algorithm 2) with a grid-based black box optimizer applied to the approximation of the operator in (42) based on the Sine-Gordon-type equation in (41) in the case $d = 1$. *Left*: Test errors of the base models prior to training as a function of the parameters used for initialization. *Right*: Test errors of the trained base models as a function of the parameters used for initialization.

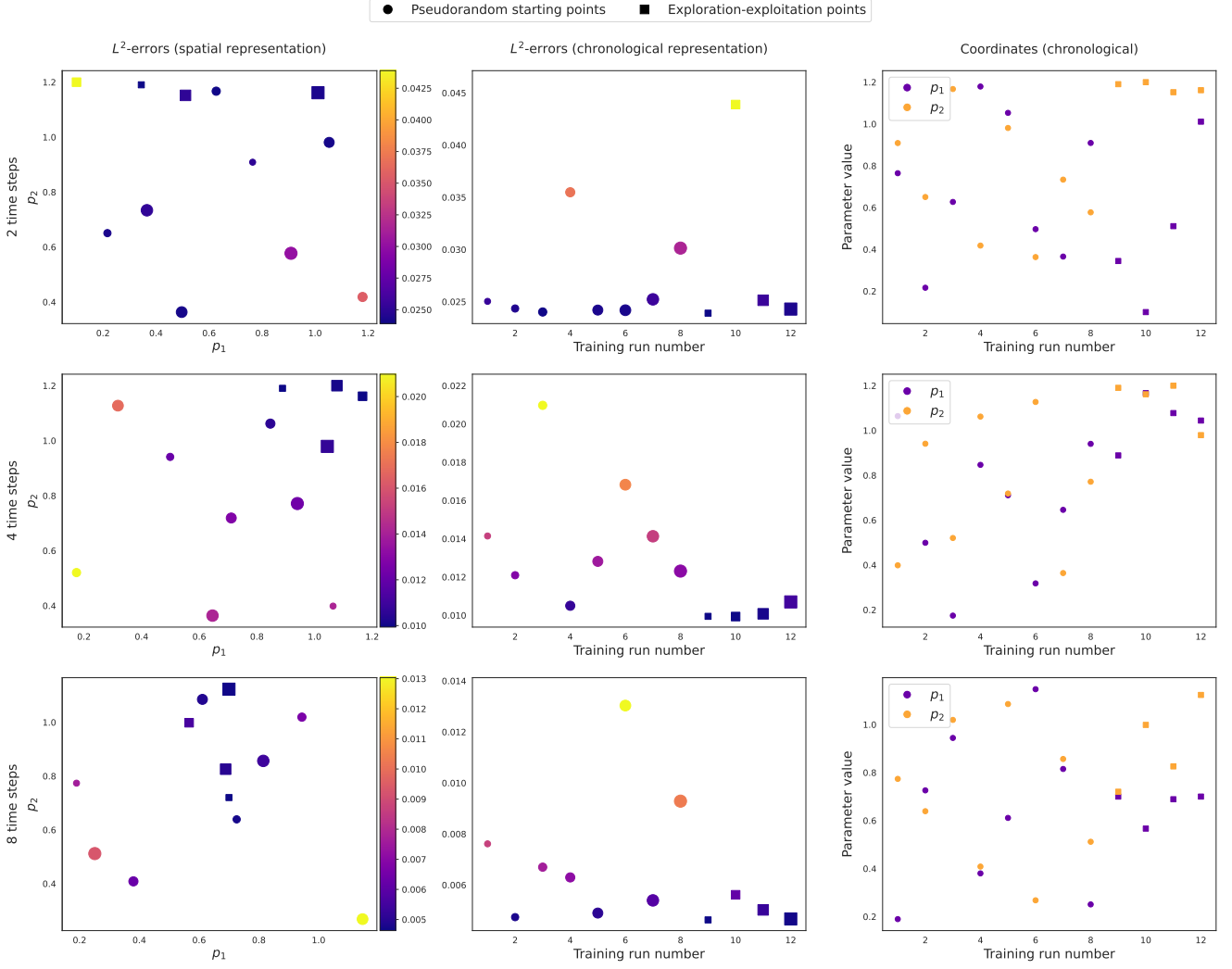


Figure 4: Illustration of the **ADANN** methodology without difference model (cf. Algorithm 2) with our heuristic exploration-exploitation black box optimizer applied to the approximation of the operator in (42) mapping initial values to terminal values of the Sine-Gordon-type equation in (41) in the case $d = 1$. *Left*: Test errors of trained base models as a function of the parameters used for initialization. Increasing scatter sizes indicate higher training run numbers. *Middle*: The same test errors represented in the order in which they appeared in the black box optimization process. *Right*: Coordinates of the chosen parameters in the black box optimization process.

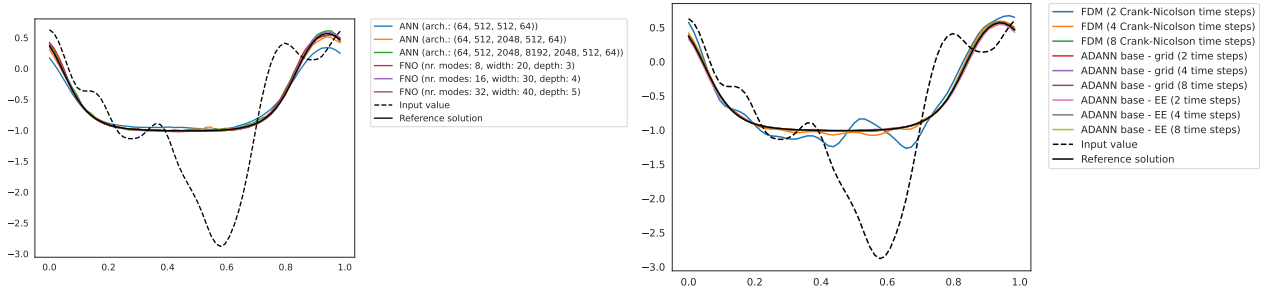


Figure 5: Example approximation plots for a randomly chosen initial value for the Sine-Gordon-type equation in (41) in the case $d = 1$. *Left*: **ANN** and **FNO** approximations. *Right*: Classical and **ADANN** approximations.

Method	Estimated L^2 -error in (44)	Average evaluation time for 2^{11} test samples over 1000 runs (in s)	Number of trainable parameters	Precomputation time (in s)
ANN (arch.: (1024, 2048, 2048, 1024))	0.157601	0.0017	8393728	580
ANN (arch.: (1024, 2048, 4096, 2048, 1024))	0.140813	0.0042	20980736	670
ANN (arch.: (1024, 2048, 4096, 8192, 4096, 2048, 1024))	0.116447	0.0168	88101888	1963
FNO (nr. modes: 8, width: 20, depth: 3)	0.044198	0.0471	108545	2270
FNO (nr. modes: 16, width: 30, depth: 4)	0.037327	0.0705	1056935	2543
FNO (nr. modes: 32, width: 40, depth: 5)	0.030493	0.1319	8733745	3174
FDM (2 Crank-Nicolson time steps)	0.337037	0.0027	0	0
FDM (4 Crank-Nicolson time steps)	0.081395	0.0055	0	0
FDM (8 Crank-Nicolson time steps)	0.029860	0.0111	0	0
ADANN base - EE (2 time steps)	0.045824	0.0027	10485760	839
ADANN base - EE (4 time steps)	0.018296	0.0055	20971520	1290
ADANN base - EE (8 time steps)	0.006498	0.0112	41943040	2002

Table 2: Comparison of the performance of different methods for the approximation of the operator in (42) mapping initial values to terminal values of the Sine-Gordon-type equation in (41) in the case $d = 2$.

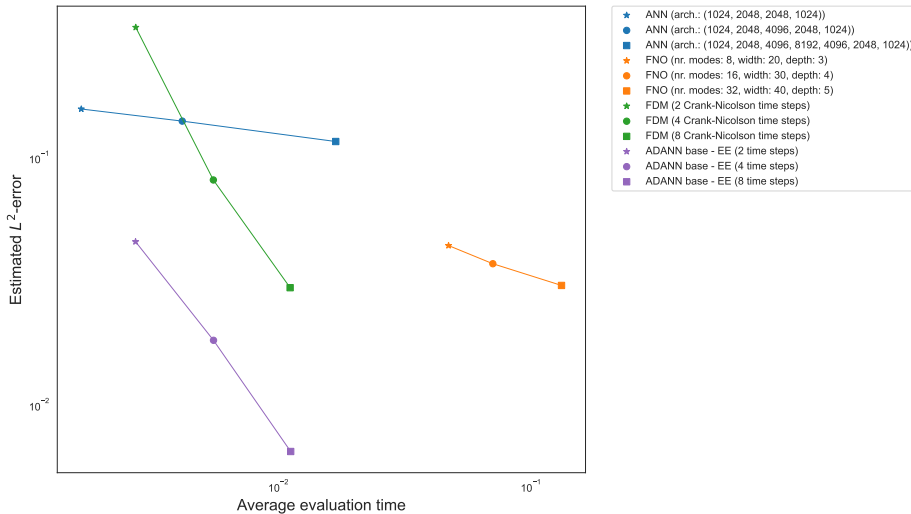


Figure 6: Graphical illustration of the performance of the methods in Table 2.

4.2.3 Numerical results for the two-dimensional Sine-Gordon-type equation

In this section we present numerical results for the approximation of the operator in (42) in the case $d = 2$. We test the ADANN methodology without difference model (cf. Algorithm 2) with the base model and the corresponding initializations defined in Section 4.3.1, space discretization $N = 32$, number of time steps $M \in \{2, 4, 8\}$, and our heuristic exploration-exploitation black box optimizer as described in Section 4.1.2 (see rows 10-12 in Table 2 and Figure 7). We also test different ANN models with GELU activation function (see rows 1-3 in Table 2), FNO models (see rows 4-6 in Table 2), and classical methods (see rows 7-9 in Table 2) for comparison. As classical methods we use the untrained base model $\mathcal{B}\mathbf{w}_{(0.5,0.5)}$ with $M \in \{2, 4, 8\}$ time steps, corresponding, roughly speaking, to a finite difference discretization in space and a Crank–Nicolson explicit midpoint LIRK discretization in time (cf. Appendix B.3). The performance of all considered methods are summarized in Table 2 and graphically illustrated in Figure 6. In addition, some of the approximations for a randomly chosen test sample are shown in Figure 8.

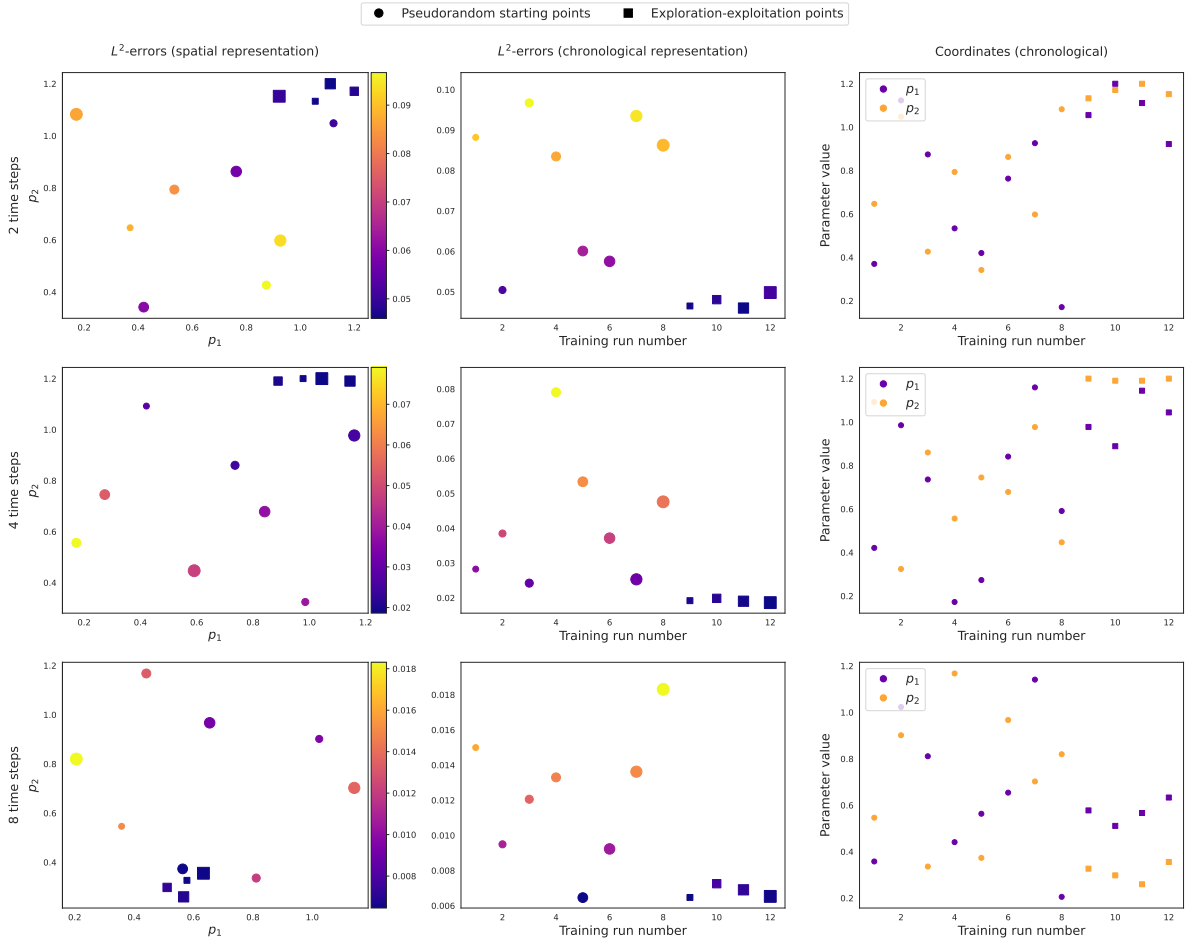


Figure 7: Illustration of the **ADANN** methodology without difference model (cf. Algorithm 2) with our heuristic exploration-exploitation black box optimizer applied to the approximation of the operator in (42) mapping initial values to terminal values of the Sine-Gordon-type equation in (41) in the case $d = 2$. *Left*: Test errors of trained base models as a function of parameters used for initialization. Increasing scatter sizes indicate higher training run numbers. *Middle*: The same test errors represented in the order in which they appeared in the black box optimization process. *Right*: Coordinates of the chosen parameters in the black box optimization process.

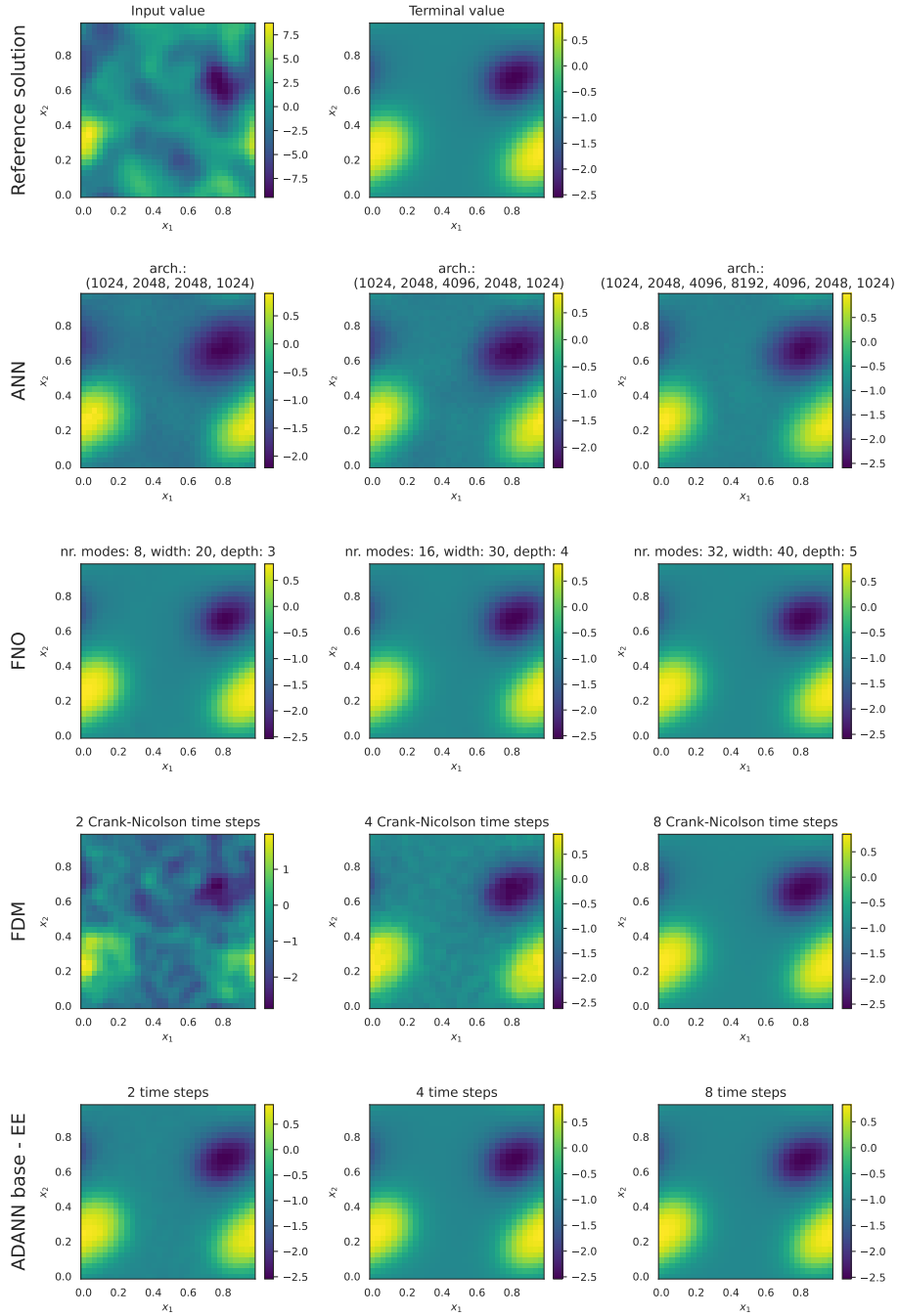


Figure 8: Example approximation plots for a randomly chosen initial value for the Sine-Gordon-type equation in (41) in the case $d = 2$.

4.3 Viscous Burgers equation

In this section we test the **ADANN** methodology as described in Section 2.4 (cf. Algorithms 1 and 2) in the case of an operator mapping initial values to terminal values of the viscous Burgers equation. We introduce below the viscous Burgers equation in conservative form and the corresponding operator. The base model for the **ADANN** methodology is defined in Section 4.3.1 and the results of our numerical simulations are presented in Section 4.3.2.

Throughout Section 4.3 assume the mathematical setting developed in Section 2, let $T = 1$, $c = \frac{1}{10}$, for every $g \in H_{\text{per}}^2((0, 2\pi); \mathbb{R})$ let $u_g: [0, T] \rightarrow H_{\text{per}}^2((0, 2\pi); \mathbb{R})$ be a mild solution of the **PDE**

$$\left(\frac{\partial}{\partial t} u_g\right)(t, x) = c(\Delta_x u_g)(t, x) - \frac{1}{2}\left(\frac{\partial}{\partial t} u_g^2\right)(t, x), \quad (t, x) \in [0, T] \times (0, 2\pi), \quad u_g(0) = g \quad (53)$$

with periodic boundary conditions, assume $\mathcal{I} = \mathcal{O} = H_{\text{per}}^2((0, 2\pi); \mathbb{R})$, and assume that the operator $\mathcal{S}: \mathcal{I} \rightarrow \mathcal{O}$ we want to approximate is given for all $g \in \mathcal{I}$ by

$$\mathcal{S}(g) = u_g(T). \quad (54)$$

Moreover, assume that the initial value $\mathfrak{J}: \Omega \rightarrow \mathcal{I}$ is $\mathcal{N}(0, 10^6(10 \text{id}_{\mathcal{I}} - \Delta_x)^{-6})$ -distributed where Δ_x is the Laplace operator on $L^2((0, 2\pi); \mathbb{R})$ with periodic boundary conditions, fix a space discretization $N = 32$, and assume for all $h \in \mathcal{O}$ that

$$\|h\|^2 = \frac{2\pi}{N} \left[\sum_{\mathfrak{r} \in \{\frac{0}{N}, \frac{1}{N}, \dots, \frac{N-1}{N}\}} (h(2\pi\mathfrak{r}))^2 \right] \approx \int_0^{2\pi} (h(x))^2 dx. \quad (55)$$

Recall that our goal is to find an approximation $\tilde{\mathcal{S}}: \mathcal{I} \rightarrow \mathcal{O}$ of the operator in (54) which minimizes the L^2 -error $\mathfrak{E}(\tilde{\mathcal{S}}) \in [0, \infty]$ given by

$$\mathfrak{E}(\tilde{\mathcal{S}}) = (\mathbb{E}[\|\tilde{\mathcal{S}}(\mathfrak{J}) - \mathcal{S}(\mathfrak{J})\|^2])^{1/2} \approx \left(\mathbb{E} \left[\int_0^{2\pi} (\tilde{\mathcal{S}}(\mathfrak{J})(x) - u_{\mathfrak{J}}(T, x))^2 dx \right] \right)^{1/2}. \quad (56)$$

4.3.1 Base model for the viscous Burgers equation

We now describe the base model that we use in the **ADANN** methodology to approximate the operator in (54). Roughly speaking, we use the same base model architecture as in Section 3.3 but we additionally integrate the first order derivative operator coming from the nonlinearity into the learnable parameters of the model. A graphical illustration for this base model can be found in Figure 1.

More precisely, let $M \in \mathbb{N}$, let $\mathbf{e}: \mathcal{I} \rightarrow \mathbb{R}^N$ be the evaluation operator on the grid $\{\frac{0}{N}, \frac{2\pi}{N}, \dots, \frac{2\pi(N-1)}{N}\}$ and let $\mathbf{i}: \mathbb{R}^N \rightarrow \mathcal{O}$ be a corresponding interpolation operator (cf. (14) and (24)), let $f: \mathbb{R} \rightarrow \mathbb{R}$ satisfy for all $x \in \mathbb{R}$ that $f(x) = -\frac{1}{2}x^2$, and assume that $\mathbf{d}_{\text{Base}} = 5N^2M$. We then assume⁸ that the base model $\mathcal{B}: ((\mathbb{R}^{N \times N})^5)^M \times \mathcal{I} \rightarrow \mathcal{O}$ is given for all $W = ((W_{m,i})_{i \in \{1,2,\dots,5\}})_{m \in \{1,2,\dots,M\}} \in ((\mathbb{R}^{N \times N})^5)^M$, $g \in \mathcal{I}$, $U_0, U_1, \dots, U_M \in \mathbb{R}^N$ with $U_0 = \mathbf{e}(g)$ and $\forall m \in \{1, 2, \dots, M\}$:

$$U_m = W_{m,1}U_{m-1} + W_{m,2}f(U_{m-1}) + W_{m,3}f(W_{m,4}U_{m-1} + W_{m,5}f(U_{m-1})) \quad (57)$$

by

$$\mathcal{B}_W(g) = \mathbf{i}(U_M). \quad (58)$$

To define the family of initialization parameters $\mathbf{W}_p \in ((\mathbb{R}^{N \times N})^5)^M$, $p \in \mathfrak{P}$, for the base model let $H = T/M$, let $I \in \mathbb{R}^{N \times N}$ be the identity matrix, let $A \in \mathbb{R}^{N \times N}$ be the finite difference discretization of the Laplace operator on $(0, 2\pi)$ with periodic boundary conditions corresponding to the evaluation

⁸In order to structure the parameters of the base model, we slightly abuse the notation and identify $\mathbb{R}^{\mathbf{d}_{\text{Base}}} \simeq ((\mathbb{R}^{N \times N})^5)^M$.

operator \mathbf{e} (cf. (15) for the definition of A for the domain $[0, 1]$), let $E \in \mathbb{R}^{N \times N}$ be the finite difference discretization of the first order derivative operator with periodic boundary conditions on $(0, 2\pi)$ given by

$$E = \frac{2\pi}{2} \begin{pmatrix} 0 & 1 & 0 & 0 & \cdots & 0 & 0 & -1 \\ -1 & 0 & 1 & 0 & \cdots & 0 & 0 & 0 \\ 0 & -1 & 0 & 1 & \cdots & 0 & 0 & 0 \\ & & & & \ddots & & & \\ 0 & 0 & 0 & 0 & \cdots & -1 & 0 & 1 \\ 1 & 0 & 0 & 0 & \cdots & 0 & -1 & 0 \end{pmatrix} \in \mathbb{R}^{N \times N}, \quad (59)$$

assume $\mathfrak{P} = (0.1, 1)^2$, and for every $p = (p_1, p_2) \in \mathfrak{P}$ let $\mathbf{w}_p = (\mathbf{w}_{p,i})_{i \in \{1,2,\dots,5\}} \in (\mathbb{R}^{N \times N})^5$ satisfy

$$\mathbf{w}_{p,1} = (I - Hp_2cA)^{-1}(I + H(1 - p_2)cA) + H^2(\frac{1}{2} - p_2)[(I - Hp_2cA)^{-1}cA]^2, \quad (60)$$

$$\mathbf{w}_{p,2} = \left[H(1 - \frac{1}{2p_1})(I - Hp_2cA)^{-1} + H^2(\frac{1}{2} - p_2)(I - Hp_2cA)^{-1}cA(I - Hp_2cA)^{-1} \right] E, \quad (61)$$

$$\mathbf{w}_{p,3} = H(\frac{1}{2p_1})(I - Hp_2cA)^{-1}E, \quad \mathbf{w}_{p,4} = (I - Hp_2cA)^{-1}(I + H(p_1 - p_2)cA), \quad (62)$$

$$\text{and} \quad \mathbf{w}_{p,5} = Hp_1(I - Hp_2cA)^{-1}E. \quad (63)$$

We then assume that for every $p \in \mathfrak{P}$ the parameters $\mathbf{W}_p \in ((\mathbb{R}^{N^d \times N^d})^5)^M$ are given by

$$\mathbf{W}_p = \underbrace{(\mathbf{w}_p, \dots, \mathbf{w}_p)}_{M\text{-times}}. \quad (64)$$

Roughly speaking, for every $p \in \mathfrak{P}$ we have that

$$\mathcal{B}_{\mathbf{w}_p} \approx \mathcal{S} \quad (65)$$

corresponds to an approximation of the viscous Burgers equation in (53) based on a finite difference discretization in space and a LIRK discretization in time where the parameter p corresponds to the parameters of the LIRK method (cf. Appendix B).

4.3.2 Numerical results for the viscous Burgers equation

In this section we present numerical results for the approximation of the operator in (54). We test the ADANN methodology with (see rows 13–15 in Table 3 and Figure 10) and without difference model (see rows 10–12 in Table 3 and Figure 10) with the base model and the corresponding initializations defined in Section 4.3.1, parameter space $\mathfrak{P} = (0.1, 1)^2$, space discretization $N = 32$, number of time steps $M \in \{2, 4, 8\}$, grid based black box optimizer as described in Section 4.1.1, and difference model given by an ANN with architecture (32, 256, 1024, 256, 32). We also test different ANN models with GELU activation function (see rows 1–3 in Table 3), FNO models (see rows 4–6 in Table 3), and classical methods (see rows 7–9 in Table 3) for comparison. As classical methods we use the untrained base model $\mathcal{B}_{\mathbf{w}_{(0.5,0.5)}}$ with $M \in \{2, 4, 8\}$ time steps, corresponding, roughly speaking, to a finite difference discretization in space and a Crank–Nicolson explicit midpoint LIRK discretization in time (cf. Appendix B.3). The performance of all considered methods is summarized in Table 3 and graphically illustrated in Figure 9. In addition, some of the approximations for a randomly chosen test sample are shown in Figure 11.

Method	Estimated L^2 -error in (56)	Average evaluation time for 2^{14} test samples over 1000 runs (in s)	Number of trainable parameters	Precomputation time (in s)
ANN (arch.: (32, 128, 512, 128, 32))	0.012470	0.0005	140064	1127
ANN (arch.: (32, 256, 1024, 256, 32))	0.010037	0.0012	542240	1145
ANN (arch.: (32, 256, 1024, 4096, 1024, 256, 32))	0.014515	0.0137	8935968	809
FNO (nr. modes: 8, width: 20, depth: 3)	0.002625	0.0130	24545	2464
FNO (nr. modes: 16, width: 30, depth: 4)	0.001570	0.0218	84935	2766
FNO (nr. modes: 32, width: 40, depth: 5)	0.001380	0.0301	301745	2917
FDM (4 Crank-Nicolson time steps)	0.024986	0.0016	0	0
FDM (8 Crank-Nicolson time steps)	0.009617	0.0031	0	0
FDM (16 Crank-Nicolson time steps)	0.010304	0.0063	0	0
ADANN base - grid (4 time steps)	0.012532	0.0017	20480	1013
ADANN base - grid (8 time steps)	0.002891	0.0031	40960	1980
ADANN base - grid (16 time steps)	0.001796	0.0062	81920	2733
ADANN full - grid (4 time steps)	0.006649	0.0019	562720	1784
ADANN full - grid (8 time steps)	0.002140	0.0035	583200	2525
ADANN full - grid (16 time steps)	0.001791	0.0066	624160	3030

Table 3: Comparison of the performance of different methods for the approximation of the operator in (54) mapping initial values to terminal values of the viscous Burgers equation in (53).

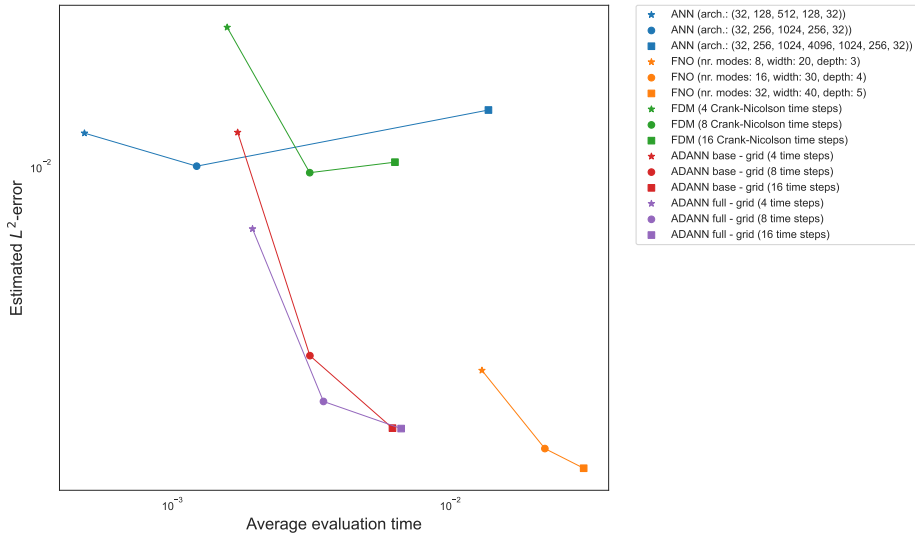


Figure 9: Graphical illustration of the performance of the methods in Table 3.

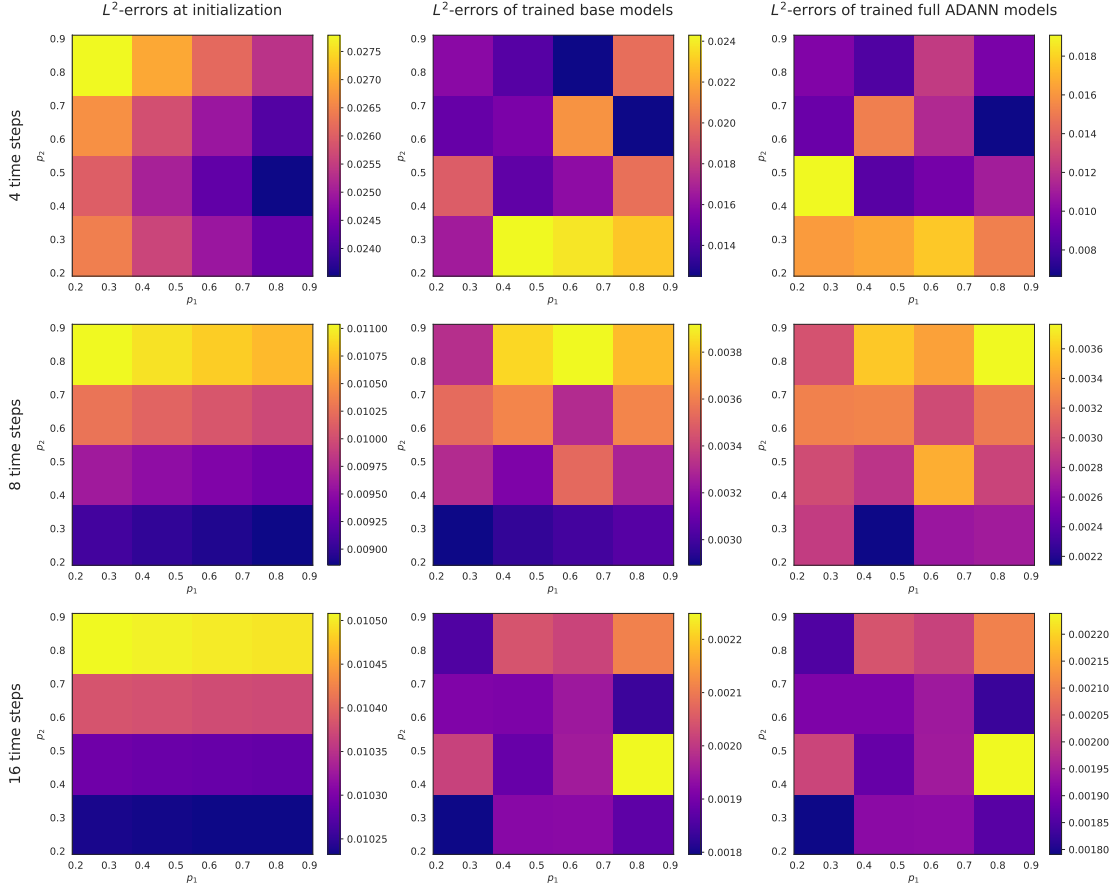


Figure 10: Illustration of the ADANN methodology with and without difference model (cf. Algorithms 1 and 2) applied to the approximation of the operator in (54) mapping initial values to terminal values of the viscous Burgers equation in (53). *Left*: Test errors of the base models prior to training as a function of the parameters used for initialization. *Middle*: Test errors of the trained base models as a function of the parameters used for initialization. *Right*: Test errors of the trained full ADANN models as a function of the parameters used for initialization of the base model.

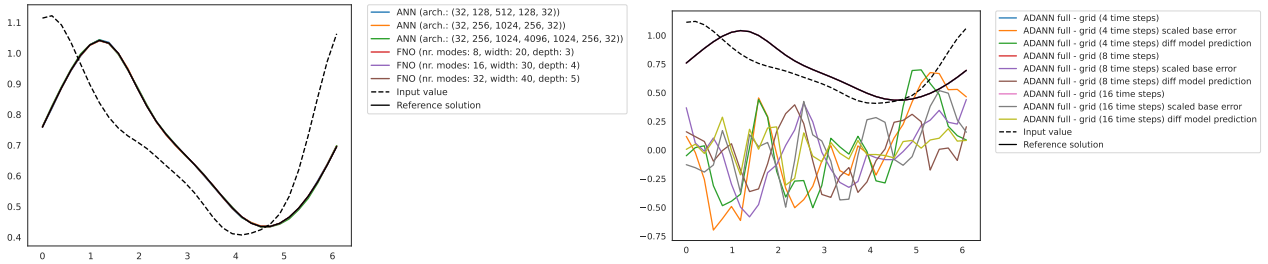


Figure 11: Example approximation plots for a randomly chosen initial value for the viscous Burgers equation in (53). *Left*: ANN and FNO approximations. *Right*: ADANN approximations.

4.4 Reaction diffusion equation

In this section we apply the **ADANN** methodology as described in Section 2.4 (cf. Algorithms 1 and 2) in the case of an operator mapping source terms to terminal values of a reaction diffusion equation. The considered operator is inspired by the reaction diffusion equation in Section 4.3 in [63]. We introduce below the considered reaction diffusion equation and the corresponding operator. The base model for the **ADANN** methodology is defined in Section 4.4.1 and the results of our numerical simulations are presented in Section 4.4.2.

Throughout Section 4.4 assume the mathematical setting developed in Section 2, let $T = 1$, $c = \frac{5}{100}$, $k = 2$, for every $g \in H_{\text{per}}^2((0, 1); \mathbb{R})$ let $u_g: [0, T] \rightarrow H_{\text{per}}^2((0, 1); \mathbb{R})$ be a mild solution of the PDE

$$\left(\frac{\partial}{\partial t} u_g\right)(t, x) = c(\Delta_x u_g)(t, x) + k(u_g(t, x) - (u_g(t, x))^3) + g(x), \quad (66)$$

$$(t, x) \in [0, T] \times (0, 1), \quad u_g(0) = 0 \quad (67)$$

with periodic boundary conditions, assume $\mathcal{I} = \mathcal{O} = H_{\text{per}}^2((0, 1); \mathbb{R})$, and assume that the operator $\mathcal{S}: \mathcal{I} \rightarrow \mathcal{O}$ we want to approximate is given for all $g \in \mathcal{I}$ by

$$\mathcal{S}(g) = u_g(T). \quad (68)$$

Moreover, assume that the source term $\mathfrak{J}: \Omega \rightarrow \mathcal{I}$ is $\mathcal{N}(0, 10^8(100 \text{id}_{\mathcal{I}} - \Delta_x)^{-4} - 0.8 \text{id}_{\mathcal{I}})$ -distributed where Δ_x is the Laplace operator on $L^2((0, 1); \mathbb{R})$ with periodic boundary conditions, fix a space discretization $N = 128$, and assume for all $h \in \mathcal{O}$ that

$$\|h\|^2 = \frac{1}{N} \left[\sum_{\mathfrak{r} \in \{\frac{0}{N}, \frac{1}{N}, \dots, \frac{N-1}{N}\}} (h(\mathfrak{r}))^2 \right] \approx \int_0^1 (h(x))^2 dx. \quad (69)$$

Recall that our goal is to find an approximation $\tilde{\mathcal{S}}: \mathcal{I} \rightarrow \mathcal{O}$ of the operator in (1) which minimizes the L^2 -error $\mathfrak{E}(\tilde{\mathcal{S}}) \in [0, \infty]$ given by

$$\mathfrak{E}(\tilde{\mathcal{S}}) = (\mathbb{E}[\|\tilde{\mathcal{S}}(\mathfrak{J}) - \mathcal{S}(\mathfrak{J})\|^2])^{1/2} \approx \left(\mathbb{E} \left[\int_0^1 (\tilde{\mathcal{S}}(\mathfrak{J})(x) - u_{\mathfrak{J}}(T, x))^2 dx \right] \right)^{1/2}. \quad (70)$$

4.4.1 Base model for the reaction diffusion equation

We now describe the base model that we use in the **ADANN** methodology to approximate the operator in (68). Very roughly speaking, we use a similar approach as in Section 3.3 to define the base model with the adjustment that the initial value is fixed and the source term is involved in every layer through additional learnable parameters. A graphical illustration for this base model can be found in Figure 12.

More precisely, let $M \in \mathbb{N}$, let $\mathbf{e}: \mathcal{I} \rightarrow \mathbb{R}^N$ be the evaluation operator on the grid $\{\frac{0}{N}, \frac{1}{N}, \dots, \frac{N-1}{N}\}$ and let $\mathbf{i}: \mathbb{R}^N \rightarrow \mathcal{O}$ be a corresponding interpolation operator (cf. (14) and (24)), let $f: \mathbb{R} \rightarrow \mathbb{R}$ satisfy for all $x \in \mathbb{R}$ that $f(x) = k(x - x^3)$, and assume that $\mathbf{d}_{\text{Base}} = 7N^2M$. We then assume⁹ that the base model $\mathcal{B}: ((\mathbb{R}^{N \times N})^7)^M \times \mathcal{I} \rightarrow \mathcal{O}$ satisfies for all $W = ((W_{m,i})_{i \in \{1,2,\dots,7\}})_{m \in \{1,2,\dots,M\}} \in ((\mathbb{R}^{N \times N})^7)^M$, $g \in \mathcal{I}$, $U_0, U_1, \dots, U_M \in \mathbb{R}^N$ with $U_0 = 0$, $\mathbf{g} = \mathbf{e}(g)$, and $\forall m \in \{1, 2, \dots, M\}$:

$$U_m = W_{m,1}U_{m-1} + W_{m,2}f(U_{m-1}) + W_{m,6}\mathbf{g} + W_{m,3}f(W_{m,4}U_{m-1} + W_{m,5}f(U_{m-1}) + W_{m,7}\mathbf{g}) \quad (71)$$

that

$$\mathcal{B}_W(g) = \mathbf{i}(U_M). \quad (72)$$

To define the family of initialization parameters $\mathbf{W}_p \in ((\mathbb{R}^{N \times N})^7)^M$, $p \in \mathfrak{P}$, for the base model let $H = T/M$, let $I \in \mathbb{R}^{N \times N}$ be the identity matrix, let $A \in \mathbb{R}^{N \times N}$ be the finite difference discretization of the Laplace operator on $(0, 1)$ with periodic boundary conditions corresponding to the evaluation

⁹In order to structure the parameters of the base model, we slightly abuse the notation and identify $\mathbb{R}^{\mathbf{d}_{\text{Base}}} \simeq ((\mathbb{R}^{N \times N})^7)^M$.

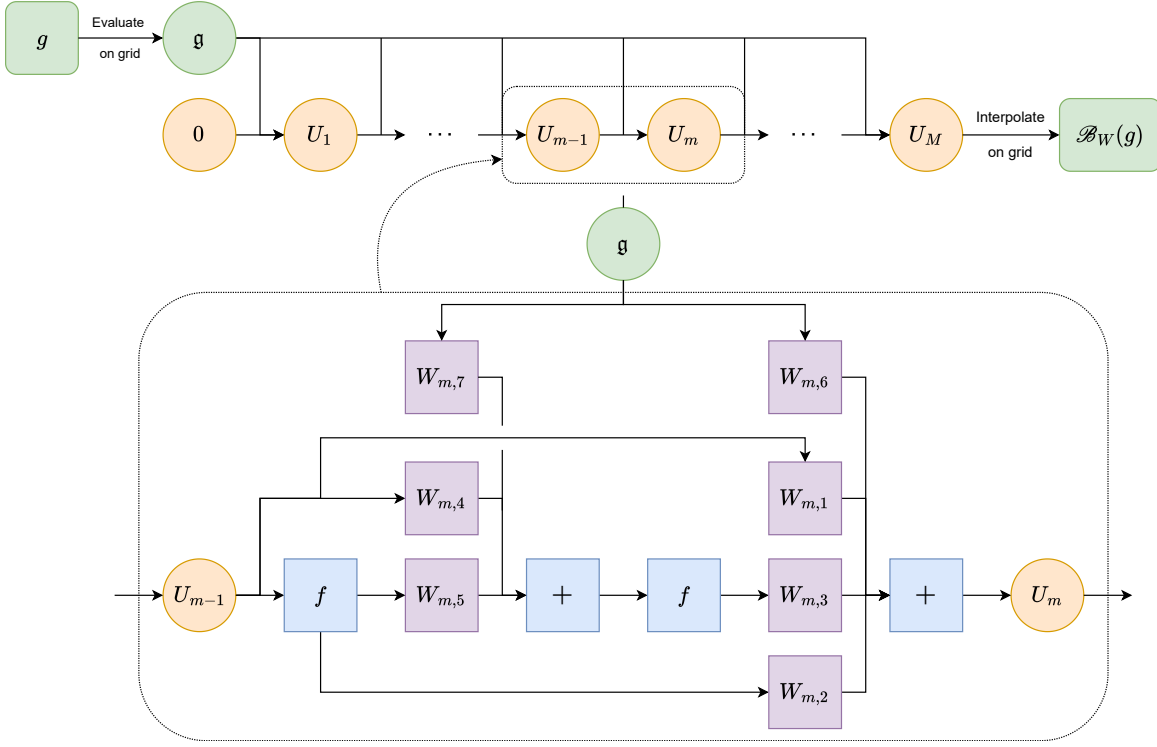


Figure 12: Graphical illustration for the base model defined in (71) and (72).

operator \mathbf{e} (cf. (15) for the definition of A), assume $\mathfrak{P} = (0.1, 1.3)^2$, and for every $p = (p_1, p_2) \in \mathfrak{P}$ let $\mathbf{w}_p = (\mathbf{w}_{p,i})_{i \in \{1,2,\dots,7\}} \in (\mathbb{R}^{N \times N})^7$ satisfy

$$\mathbf{w}_{p,1} = (I - Hp_2cA)^{-1}(I + H(1 - p_2)cA) + H^2(\frac{1}{2} - p_2)[(I - Hp_2cA)^{-1}cA]^2, \quad (73)$$

$$\mathbf{w}_{p,2} = H(1 - \frac{1}{2p_1})(I - Hp_2cA)^{-1} + H^2(\frac{1}{2} - p_2)(I - Hp_2cA)^{-1}cA(I - Hp_2cA)^{-1}, \quad (74)$$

$$\mathbf{w}_{p,3} = H(\frac{1}{2p_1})(I - Hp_2cA)^{-1}, \quad \mathbf{w}_{p,4} = (I - Hp_2cA)^{-1}(I + H(p_1 - p_2)cA), \quad (75)$$

$$\mathbf{w}_{p,5} = Hp_1(I - Hp_2cA)^{-1}, \quad \mathbf{w}_{p,6} = \mathbf{w}_{p,2} + \mathbf{w}_{p,3}, \quad \text{and} \quad \mathbf{w}_{p,7} = \mathbf{w}_{p,5}. \quad (76)$$

We then assume that for every $p \in \mathfrak{P}$ the parameters $\mathbf{W}_p \in ((\mathbb{R}^{N^d \times N^d})^7)^M$ are given by

$$\mathbf{W}_p = \underbrace{(\mathbf{w}_p, \dots, \mathbf{w}_p)}_{M\text{-times}}. \quad (77)$$

Roughly speaking, for every $p \in \mathfrak{P}$ we have that

$$\mathcal{B}_{\mathbf{W}_p} \approx \mathcal{S} \quad (78)$$

corresponds to an approximation of the reaction diffusion equation in (66) based on a finite difference discretization in space and a LIRK discretization in time where the parameters p correspond to the parameters of the LIRK method (cf. Appendix B).

4.4.2 Numerical results for the reaction diffusion equation

In this section we present numerical results for the approximation of the operator in (68). We test the ADANN methodology with (see rows 13–15 in Table 4 and Figure 14) and without difference model (see rows 10–12 in Table 4 and Figure 14) with the base model and the corresponding initializations defined in Section 4.4.1, parameter space $\mathfrak{P} = (0.1, 1.3)^2$, space discretization $N = 128$, number of time steps $M \in \{2, 4, 8\}$, grid based black box optimizer as described in Section 4.1.1, and difference model given by an ANN with architecture (128, 512, 1024, 512, 128). We also test different ANN models with GELU activation function (see rows 1-3 in Table 4), FNO models (see rows 4-6 in Table 4), and classical methods

Method	Estimated L^2 -error	Average evaluation time for 2^{14} test samples over 1000 runs (in s)	Number of trainable parameters	Precomputation time (in s)
ANN (arch.: (128, 512, 1024, 512, 128))	0.003317	0.0022	1181824	1024
ANN (arch.: (128, 1024, 4096, 1024, 128))	0.002747	0.0127	8657024	1079
ANN (arch.: (128, 1024, 4096, 8192, 4096, 1024, 128))	0.002721	0.1092	75778176	2838
FNO (nr. modes: 8, width: 20, depth: 3)	0.002986	0.0421	24545	3402
FNO (nr. modes: 16, width: 30, depth: 4)	0.001708	0.0570	84935	4478
FNO (nr. modes: 32, width: 40, depth: 5)	0.001606	0.0786	301745	5529
FDM (4 Crank-Nicolson time steps)	0.032469	0.0026	0	0
FDM (8 Crank-Nicolson time steps)	0.004785	0.0052	0	0
FDM (16 Crank-Nicolson time steps)	0.001153	0.0103	0	0
ADANN base - grid (4 time steps)	0.000872	0.0027	458752	2588
ADANN base - grid (8 time steps)	0.000352	0.0052	917504	3318
ADANN base - grid (16 time steps)	0.000095	0.0104	1835008	4706
ADANN full - grid (4 time steps)	0.000198	0.0050	1640576	3234
ADANN full - grid (8 time steps)	0.000043	0.0076	2099328	4214
ADANN full - grid (16 time steps)	0.000021	0.0128	3016832	5485

Table 4: Comparison of the performance of different methods for the approximation of the operator in (68) mapping source terms to terminal values of the reaction diffusion equation in (66).

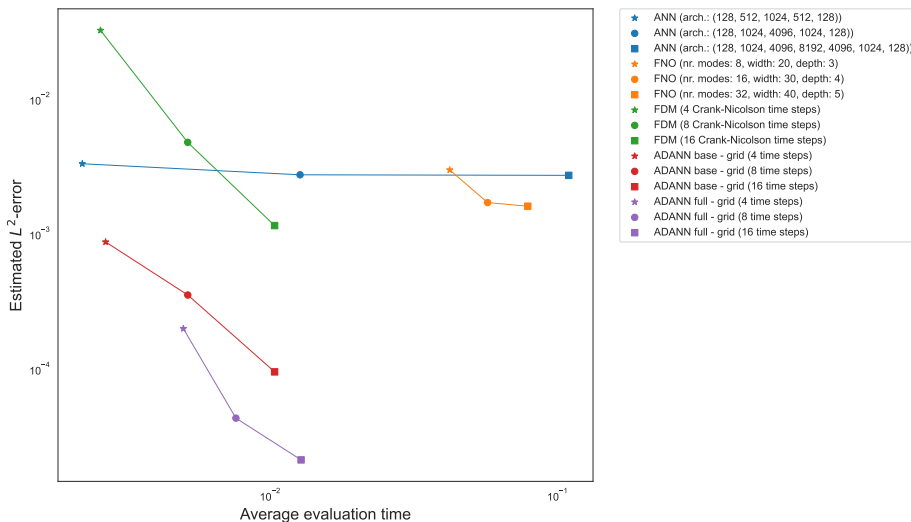


Figure 13: Graphical illustration of the performance of the methods in Table 4.

(see rows 7-9 in Table 4) for comparison. As classical methods we use the untrained base model $\mathcal{B}\mathbf{w}_{(0.5,0.5)}$ with $M \in \{2, 4, 8\}$ time steps, corresponding, roughly speaking, to a finite difference discretization in space and a Crank–Nicolson explicit midpoint LIRK discretization in time (cf. Appendix B.3). The performance of all considered methods are summarized in Table 4 and graphically illustrated in Figure 13. In addition, some of the approximations for a randomly chosen test sample are shown in Figure 15.

5 Conclusion and future work

In this article we introduced the ADANN methodology, a general framework which combines classical numerical algorithms with operator learning techniques. We demonstrated its effectiveness in the context of several operators related to nonlinear parabolic PDEs, showing that the ADANN methodology can outperform both classical numerical algorithms and other operator learning techniques. There are a number of directions for further research arising from this work. One natural direction is to apply the ADANN methodology to other types of PDE problems with different base and difference models, involving the creative design of new base models based on designing algorithms for the considered PDE problems. Another direction is to refine the optimization over base model initializations in the ADANN methodology (see Section 2.3). This could involve developing a theoretical understanding of the objective function landscape which empirically seems to exhibit a certain regularity (cf. Figures 3, 10, and 14). Finally, the ADANN methodology seems suitable for an overall error analysis as it involves classical numerical algorithms which already have a well-established theoretical foundation.

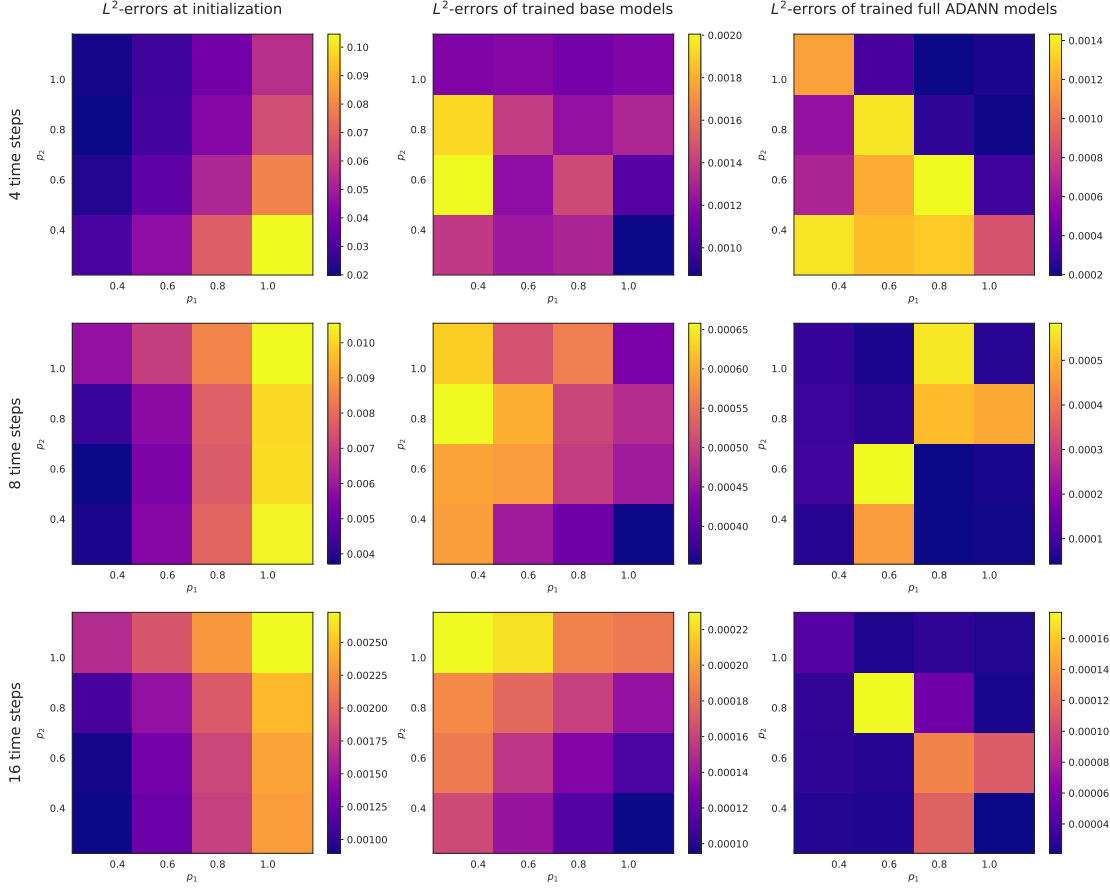


Figure 14: Illustration of the **ADANN** methodology with and without difference model (cf. Algorithms 1 and 2) applied to the approximation of the operator in (68) mapping source terms to terminal values of the reaction diffusion equation in (66). *Left*: Test errors of the base models prior to training as a function of the parameters used for initialization. *Middle*: Test errors of the trained base models as a function of the parameters used for initialization. *Right*: Test errors of the trained full **ADANN** models as a function of the parameters used for initialization of the base model.

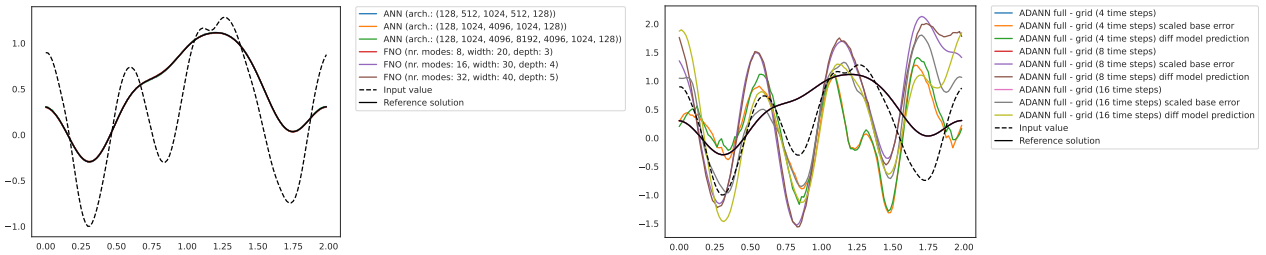


Figure 15: Example approximation plots for a randomly chosen initial value for the reaction diffusion equation in (66). *Left*: **ANN** and **FNO** approximations. *Right*: **ADANN** approximations.

Acknowledgments

This work has been partially funded by the National Science Foundation of China (NSFC) under grant number 12250610192. This work has also been partially funded by the Deutsche Forschungsgemeinschaft (DFG, German Research Foundation) under Germany's Excellence Strategy EXC 2044-390685587, Mathematics Münster: Dynamics-Geometry-Structure.

Appendix A Training

In this section we provide additional details on the training procedure used in the numerical simulations in Section 4. In the training of all models we use the Adam optimizer with adaptively chosen learning rates. Specifically, for every model and every corresponding initialization we approximately choose an optimal initial learning rate and, thereafter, during the training process, successively reduce the learning rate depending on the validation error of the model.

We discuss the method by which we optimize initial learning rates in Appendix A.1 and we provide details on the adaptive learning rate reduction in Appendix A.2. Furthermore, we list our specific choices of hyperparameters for the experiments in Section 4, including the parameters governing the choice of adaptive learning rates and those for the generation of training, validation, and test sets, in Table 5.

A.1 Optimal choice of initial learning rates

In all our numerical simulations in Section 4, in the training of every model we use for every considered initialization an approximately optimal initial learning rate for the ADAM optimizer. To select such an approximately optimal initial learning rate for a model and a corresponding initialization, we apply a golden section search (cf., e.g., [2, Section 4.4]) to minimize the function mapping a learning rate to the validation error of the model after a fixed number of ADAM training steps with that learning rate. The approximate minimum point identified through the golden section search is then used as the initial learning rate for the ADAM training process of the considered model and initialization. The use of the golden section search is justified by the empirical observation that the function mapping a learning rate to the validation error after a fixed number of training steps empirically tends to be unimodal, that is, there is a unique minimum and the function is strictly decreasing on the left and strictly increasing on the right of the minimum.

Choosing the initial learning rate adaptively in our experiments was motivated by the empirical observation that the standard initial learning rate of 0.001 for the Adam optimizer often led to no improvement or even deterioration of the validation error in the training of ADANN base models with highly specialized initializations. As an example for this observation, we provide in Figure 16 approximate optimal learning rates for the base models introduced in (45)–(46) in Section 4.2.1 with the initializations in (51) for $p = (1/2, 1/2)$. We consider different space discretizations (corresponding to the variable N in Section 4.2.1) and different time discretizations (corresponding to the variable M in Section 4.2.1) and evaluate the validation error after 50 training steps.

We observe that the approximate optimal learning rates seem to decrease as a function of the number of space steps and the number of time steps. Moreover, we note that the four plots on the right hand side in Figure 16 suggest that the function mapping a learning rate to the validation error after a fixed number of training steps is indeed approximately unimodal. Also, we observe that in the cases $N = 16$, $M = 64$ and $N = 64$, $M = 64$ (corresponding to the two plots on the lower right in Figure 16) the standard learning rate of 0.001 for the ADAM optimizer seems to lead to a clear deterioration of the validation error after 50 training steps.

A.2 Adaptive reduction of learning rates

In the training of all models in the numerical simulations in Section 4, we adaptively reduce the learning rate and abort the training process guided by the validation error of the model being trained. Specifically, during the training process of a model we evaluate the validation error every fixed number of training steps and whenever the relative improvement from the previous evaluation of the validation error is worse than a certain tolerance we divide the learning rate by the factor 5. If after a learning rate reduction, the next relative improvement of the validation error is again worse than the tolerance we abort the training process. Within every approximation problem in Section 4, the number of training steps between evaluations of the validation error and the relative improvement tolerance are chosen to be the same for all considered training procedures. The respective choices for each problem are listed in Table 5.

	Sine-Gordon ($d = 1$) (cf. Section 4.2.2)	Sine-Gordon ($d = 2$) (cf. Section 4.2.3)	Burgers (cf. Section 4.3)	Reaction diffusion (cf. Section 4.4)
# space steps per dimension (N)	64	32	32	128
Designing parameter set \mathfrak{P}	$(0.1, 1.2) \times (0.25, 1.2)$	$(0.1, 1.2) \times (0.25, 1.2)$	$(0.1, 1)^2$	$(0.1, 1.3)^2$
Training				
Batch size	256	128	1024	256
# tr. steps for init. LR search	50	50	50	50
# tr. steps between val. error eval.	400	400	400	400
Improvement tolerance	0.96	0.96	0.96	0.97
# of tr. runs per model				
ADANNs - grid	25	–	16	16
ADANNs - EE	12	12	–	–
ANNs and FNOs	12	12	16	16
Algorithm for reference sol.				
	Spectral/Crank-Nicolson explicit midpoint	Spectral/Crank-Nicolson explicit midpoint	Spectral/Crank-Nicolson explicit midpoint	FDM/Crank-Nicolson explicit midpoint
Training set				
# samples	2^{18}	2^{16}	2^{18}	2^{18}
# space steps per dimension	256	64	128	512
# time steps	1000	1000	1000	1000
Validation set				
# samples	2^{14}	2^{11}	2^{14}	2^{14}
# space steps per dimension	512	128	256	1024
# time steps	1500	1500	1500	1500
Test set				
# samples	2^{14}	2^{11}	2^{14}	2^{14}
# space steps per dimension	512	128	256	1024
# time steps	1500	1500	1500	1500

Table 5: Hyperparameters for the training of the models in the numerical simulations in Section 4.

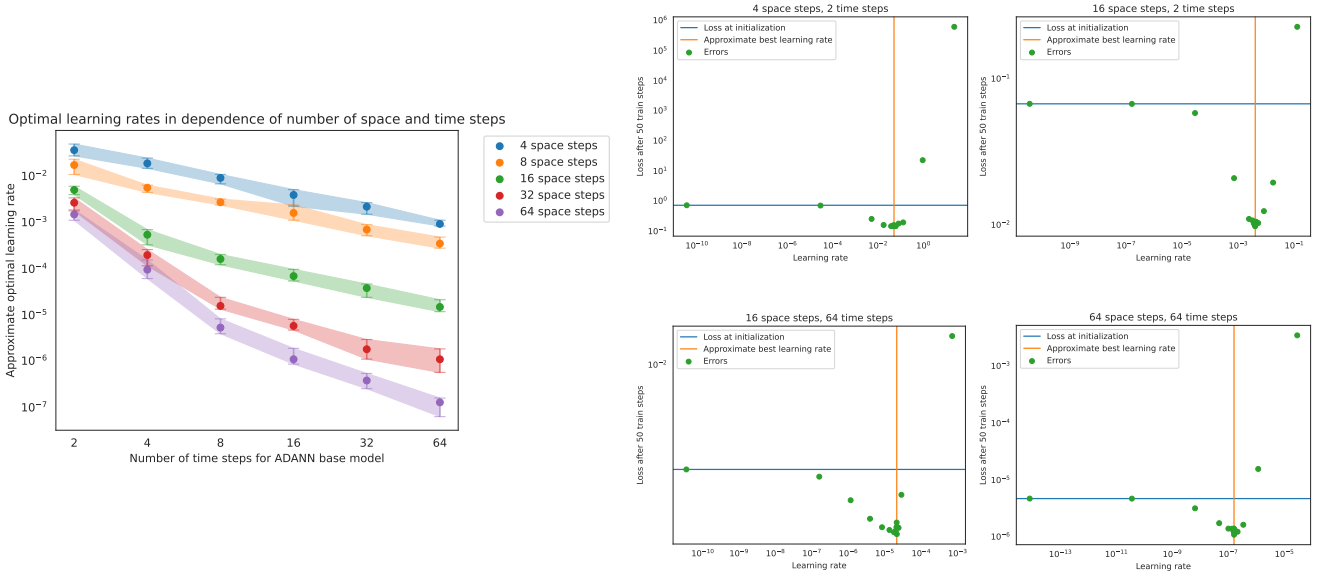


Figure 16: Optimal learning rates for the base model introduced in Section 4.2.1 for the one-dimensional Sine-Gordon-type equation. *Left*: Approximate optimal learning rates for different space discretizations and time discretizations in the base model. The scatter points represent the average of approximated optimal learning rates from 5 runs of golden section search and the error bars represent the spread over those 5 runs. *Right (4 plots)*: Some examples of the validation errors after 50 train steps computed during some of the golden section searches done for the left plot.

Appendix B Second order LIRK methods

In this section we present a formal derivation of a well-known family of second order LIRK methods for semilinear ODEs (cf., e.g., [18, Section 6.4] and [42]) which are used to construct base models and corresponding initializations in Sections 3 and 4. We will work in the following setting. Let $d \in \mathbb{N}$, $A \in \mathbb{R}^{d \times d}$, $f \in C(\mathbb{R}^d, \mathbb{R}^d)$ and consider the ODE

$$\dot{u}(t) = Au(t) + f(u(t)) \quad (79)$$

for $t \in (0, \infty)$.

B.1 Order conditions for general LIRK methods

We first introduce the one step increment function of general LIRK methods for the ODE in (79). Specifically, let $s \in \mathbb{N}$, $\alpha = (\alpha_{i,j})_{(i,j) \in \{1,2,\dots,s\}^2} \in \mathbb{R}^{s \times s}$, $\beta = (\beta_{i,j})_{(i,j) \in \{1,2,\dots,s\}^2} \in \mathbb{R}^{s \times s}$, $b = (b_i)_{i \in \{1,2,\dots,s\}} \in \mathbb{R}^s$ and let $\Phi = (\Phi^h(u))_{(h,u) \in [0,\varepsilon] \times \mathbb{R}^d} : [0,\varepsilon] \times \mathbb{R}^d \rightarrow \mathbb{R}^d$ satisfy for all $h \in [0, \infty)$, $U, k_1, k_2, \dots, k_s \in \mathbb{R}^d$ with

$$\forall i \in \{1, 2, \dots, s\}: \quad k_i = A(U + h \sum_{j=1}^i \beta_{i,j} k_j) + f(U + h \sum_{j=1}^{i-1} \alpha_{i,j} k_j) \quad (80)$$

that

$$\Phi^h(U) = U + h \sum_{i=1}^s b_i k_i. \quad (81)$$

We refer to the number s as the number of stages of the LIRK method, we refer to α as the nonlinear LIRK parameters, we refer to β as the linear LIRK parameters, we refer to b as the LIRK integration weights, and we refer to k_1, k_2, \dots, k_s as the LIRK stages. Although the LIRK stages are defined implicitly in (80), under suitable conditions they can be computed explicitly. Specifically, under suitable conditions, we have for all $h \in [0, \infty)$, $U, k_1, k_2, \dots, k_s \in \mathbb{R}^d$ with

$$\forall i \in \{1, 2, \dots, s\}: \quad k_i = (I_d - h\beta_{i,i}A)^{-1} \left(A(U + h \sum_{j=1}^{i-1} \beta_{i,j} k_j) + f(U + h \sum_{j=1}^{i-1} \alpha_{i,j} k_j) \right) \quad (82)$$

that

$$\Phi^h(U) = U + h \sum_{i=1}^s b_i k_i. \quad (83)$$

Order conditions for the one step method Φ are obtained by formally setting the Taylor expansion of Φ equal to the Taylor expansion of the solution of the ODE in (79) for a fixed initial value $U \in \mathbb{R}^d$ up to terms of a certain order. The resulting order conditions for a second order scheme are given by

$$\sum_{i=1}^s b_i = 1 \quad \text{and} \quad \sum_{i=1}^s b_i C_i = \sum_{i=1}^s b_i c_i = \frac{1}{2}, \quad (84)$$

where $(C_i)_{i \in \{1,2,\dots,s\}}, (c_i)_{i \in \{1,2,\dots,s\}} \subseteq \mathbb{R}$ satisfy for all $i \in \{1, 2, \dots, s\}$ that

$$C_i = \sum_{j=1}^i \beta_{i,j} \quad \text{and} \quad c_i = \sum_{j=1}^{i-1} \alpha_{i,j}. \quad (85)$$

Under suitable regularity on the nonlinearity f the conditions in (84) ensure that the ODE integration scheme defined through the one step increment function Φ will have global convergence order 2.

B.2 A family of 2 stage LIRK methods of order 2

In this section we solve the order conditions in (84) in the case of $s = 2$ stages and under the assumption that $\beta_{1,1} = \beta_{2,2}$. For this, let $p_1, p_2 \in (0, \infty)$ and assume that

$$\alpha_{1,2} = p_1 \quad \text{and} \quad \beta_{1,1} = \beta_{2,2} = p_2. \quad (86)$$

This and (84) imply that

$$b_1 = 1 - \frac{1}{2p_1}, \quad b_2 = \frac{1}{2p_1}, \quad \text{and} \quad \beta_{1,2} = 2p_1\left(\frac{1}{2} - p_2\right). \quad (87)$$

This and (82) in turn imply, under suitable conditions, that for all $h \in [0, \infty)$, $U, k_1, k_2 \in \mathbb{R}^d$ with

$$k_1 = (I_d - hp_2 A)^{-1}(AU + f(U)) \quad \text{and} \quad (88)$$

$$k_2 = (I_d - hp_2 A)^{-1}(A(U + h2p_1(\frac{1}{2} - p_2)k_1) + f(U + hp_1 k_1)) \quad (89)$$

it holds that

$$\Phi^h(U) = U + h\left[\left(1 - \frac{1}{2p_1}\right)k_1 + \left(\frac{1}{2p_1}\right)k_2\right]. \quad (90)$$

We have thus derived a family of LIRK methods of order two, which is parametrized by two parameters p_1 and p_2 . We use this family in Section 3.2.2.

B.3 The special case of the Crank–Nicolson explicit midpoint method

The scheme in (88)–(90) includes as a special case the well-known Crank–Nicolson explicit midpoint LIRK scheme. Specifically, note that in the special case where $p_1 = p_2 = \frac{1}{2}$ we have for all $h \in [0, \infty)$, $U \in \mathbb{R}^d$ that

$$\Phi^h(U) = (I_d - \frac{h}{2}A)^{-1}\left((I_d + \frac{h}{2}A)U + hf\left((I_d - \frac{h}{2}A)^{-1}(U + \frac{h}{2}f(u))\right)\right). \quad (91)$$

References

- [1] ANASTASSI, A. A. Constructing Runge–Kutta methods with the use of artificial neural networks. *Neural Computing and Applications* 25, 1 (2014), 229–236.
- [2] ANTONIOU, A., AND LU, W.-S. *Practical Optimization: Algorithms and Engineering Applications*. Springer US, 2021.

- [3] BAR-SINAI, Y., HOYER, S., HICKEY, J., AND BRENNER, M. P. Learning data-driven discretizations for partial differential equations. *Proc. Natl. Acad. Sci. USA* 116, 31 (2019), 15344–15349.
- [4] BARTELS, S. *Numerical Methods for Nonlinear Partial Differential Equations*. Springer International Publishing, 2015.
- [5] BECK, C., HUTZENTHALER, M., JENTZEN, A., AND KUCKUCK, B. An overview on deep learning-based approximation methods for partial differential equations. *Discrete Contin. Dyn. Syst. Ser. B* (2022) (2020).
- [6] BECKER, S., JENTZEN, A., MÜLLER, M. S., AND VON WURSTEMBERGER, P. Learning the random variables in Monte Carlo simulations with stochastic gradient descent: machine learning for parametric PDEs and financial derivative pricing. *Math. Finance* 34, 1 (2024), 90–150.
- [7] BELLMAN, R. Dynamic programming. *Science* 153, 3731 (1966), 34–37.
- [8] BLECHSCHMIDT, J., AND ERNST, O. G. Three Ways to Solve Partial Differential Equations with Neural Networks—A Review. *arXiv:2102.11802* (2021).
- [9] BOHN, J., AND FEISCHL, M. Recurrent neural networks as optimal mesh refinement strategies. *Computers & Mathematics with Applications* 97 (2021), 61–76.
- [10] BRANDSTETTER, J., BERG, R. V. D., WELLING, M., AND GUPTA, J. K. Clifford neural layers for PDE modeling. *arXiv:2209.04934* (2022).
- [11] BREVIS, I., MUGA, I., AND VAN DER ZEE, K. G. A machine-learning minimal-residual (ML-MRes) framework for goal-oriented finite element discretizations. *Computers & Mathematics with Applications* 95 (2021), 186–199. Recent Advances in Least-Squares and Discontinuous Petrov–Galerkin Finite Element Methods.
- [12] BROWN, T. B., MANN, B., RYDER, N., SUBBIAH, M., KAPLAN, J., DHARIWAL, P., NEELAKANTAN, A., SHYAM, P., SASTRY, G., ASKELL, A., AGARWAL, S., HERBERT-VOSS, A., KRUEGER, G., HENIGHAN, T., CHILD, R., RAMESH, A., ZIEGLER, D. M., WU, J., WINTER, C., HESSE, C., CHEN, M., SIGLER, E., LITWIN, M., GRAY, S., CHESSE, B., CLARK, J., BERNER, C., MCCANDLISH, S., RADFORD, A., SUTSKEVER, I., AND AMODEI, D. Language Models are Few-Shot Learners. *arXiv:2005.14165* (2020).
- [13] CAZENAVE, T., AND HARAUX, A. *An introduction to semilinear evolution equations*, vol. 13 of *Oxford Lecture Series in Mathematics and its Applications*. The Clarendon Press, Oxford University Press, New York, 1998. Translated from the 1990 French original by Yvan Martel and revised by the authors.
- [14] CHEN, K., WANG, C., AND YANG, H. Deep operator learning lessens the curse of dimensionality for PDEs. *arXiv:2301.12227* (2023).
- [15] CONN, A. R., SCHEINBERG, K., AND VICENTE, L. N. *Introduction to Derivative-Free Optimization*. Society for Industrial and Applied Mathematics, 2009.
- [16] DEHGHANPOUR, M., RAHATI, A., AND DEHGHANIAN, E. ANN-based modeling of third order runge kutta method. *Journal of Advanced Computer Science & Technology* 4, 1 (2015), 180–189.
- [17] DENG, L., LI, J., HUANG, J.-T., YAO, K., YU, D., SEIDE, F., SELTZER, M., ZWEIG, G., HE, X., WILLIAMS, J., GONG, Y., AND ACERO, A. Recent advances in deep learning for speech research at Microsoft. In *2013 IEEE International Conference on Acoustics, Speech and Signal Processing* (2013), pp. 8604–8608.
- [18] DEUFLHARD, P., AND BORNEMANN, F. *Numerische Mathematik 2*, revised ed. de Gruyter Lehrbuch. Walter de Gruyter & Co., Berlin, 2008. Gewöhnliche Differentialgleichungen.

- [19] DISCACCIATI, N., HESTHAVEN, J. S., AND RAY, D. Controlling oscillations in high-order Discontinuous Galerkin schemes using artificial viscosity tuned by neural networks. *Journal of Computational Physics* 409 (2020), 109304.
- [20] DOSOVITSKIY, A., BEYER, L., KOLESNIKOV, A., WEISSENBORN, D., ZHAI, X., UNTERTHINER, T., DEGHANI, M., MINDERER, M., HEIGOLD, G., GELLY, S., USZKOREIT, J., AND HOULSBY, N. An Image is Worth 16x16 Words: Transformers for Image Recognition at Scale. In *International Conference on Learning Representations* (2021).
- [21] DRESDNER, G., KOCHKOV, D., NORGAARD, P., ZEPEDA-NÚÑEZ, L., SMITH, J. A., BRENNER, M. P., AND HOYER, S. Learning to correct spectral methods for simulating turbulent flows. *arXiv:2207.00556* (2022).
- [22] E, W., HAN, J., AND JENTZEN, A. Deep learning-based numerical methods for high-dimensional parabolic partial differential equations and backward stochastic differential equations. *Communications in Mathematics and Statistics* 5, 4 (2017), 349–380.
- [23] E, W., HAN, J., AND JENTZEN, A. Algorithms for Solving High Dimensional PDEs: From Non-linear Monte Carlo to Machine Learning. *Nonlinearity* 35 (2022) 278-310 (2020).
- [24] E, W., HUTZENTHALER, M., JENTZEN, A., AND KRUSE, T. On multilevel Picard numerical approximations for high-dimensional nonlinear parabolic partial differential equations and high-dimensional nonlinear backward stochastic differential equations. *J. Sci. Comput.* 79, 3 (2019), 1534–1571.
- [25] E, W., HUTZENTHALER, M., JENTZEN, A., AND KRUSE, T. Multilevel Picard iterations for solving smooth semilinear parabolic heat equations. *Partial Differ. Equ. Appl.* 2, 6 (2021), 80.
- [26] ENGEL, K.-J., AND NAGEL, R. *One-parameter semigroups for linear evolution equations*, vol. 194 of *Graduate Texts in Mathematics*. Springer-Verlag, New York, 2000. With contributions by S. Brendle, M. Campiti, T. Hahn, G. Metafuno, G. Nickel, D. Pallara, C. Perazzoli, A. Rhandi, S. Romanelli and R. Schnaubelt.
- [27] FIDKOWSKI, K. J., AND CHEN, G. Metric-based, goal-oriented mesh adaptation using machine learning. *Journal of Computational Physics* 426 (2021), 109957.
- [28] FREZAT, H., LE SOMMER, J., FABLET, R., BALARAC, G., AND LGUENSAT, R. A Posteriori Learning for Quasi-Geostrophic Turbulence Parametrization. *Journal of Advances in Modeling Earth Systems* 14, 11 (Nov. 2022).
- [29] GERMAIN, M., PHAM, H., AND WARIN, X. Neural networks-based algorithms for stochastic control and PDEs in finance. *arXiv:2101.08068* (2021).
- [30] GREENFELD, D., GALUN, M., BASRI, R., YAVNEH, I., AND KIMMEL, R. Learning to optimize multigrid PDE solvers. In *Proceedings of the 36th International Conference on Machine Learning* (09–15 Jun 2019), K. Chaudhuri and R. Salakhutdinov, Eds., vol. 97 of *Proceedings of Machine Learning Research*, PMLR, pp. 2415–2423.
- [31] GROHS, P., AND VOIGTLAENDER, F. Proof of the Theory-to-Practice Gap in Deep Learning via Sampling Complexity bounds for Neural Network Approximation Spaces. *Foundations of Computational Mathematics* (Jul 2023).
- [32] GUO, X., LI, W., AND IORIO, F. Convolutional Neural Networks for Steady Flow Approximation. In *Proceedings of the 22nd ACM SIGKDD International Conference on Knowledge Discovery and Data Mining* (New York, NY, USA, 2016), KDD '16, Association for Computing Machinery, p. 481–490.
- [33] HAIRER, E., AND WANNER, G. *Solving ordinary differential equations. II*, revised ed., vol. 14 of *Springer Series in Computational Mathematics*. Springer-Verlag, Berlin, 2010. Stiff and differential-algebraic problems.

- [34] HAN, J., JENTZEN, A., AND E, W. Solving high-dimensional partial differential equations using deep learning. *Proceedings of the National Academy of Sciences* 115, 34 (2018), 8505–8510.
- [35] HEAD, T., KUMAR, M., NAHRSTAEDT, H., LOUPPE, G., AND SHCHERBATYI, I. scikit-optimize/scikit-optimize, 2021.
- [36] HEINRICH, S. The randomized information complexity of elliptic PDE. *Journal of Complexity* 22, 2 (2006), 220–249.
- [37] HEINRICH, S., AND SINDAMBIWE, E. Monte Carlo Complexity of Parametric Integration. *Journal of Complexity* 15, 3 (1999), 317–341.
- [38] HEISS, C., GÜHRING, I., AND EIGEL, M. Multilevel CNNs for parametric PDEs. *arXiv:2304.00388* (2023).
- [39] HENRY-LABORDERE, P. Counterparty Risk Valuation: A Marked Branching Diffusion Approach. *arXiv:1203.2369* (2012).
- [40] HENRY-LABORDERE, P., OUDJANE, N., TAN, X., TOUZI, N., WARIN, X., ET AL. Branching diffusion representation of semilinear pdes and monte carlo approximation. In *Annales de l'Institut Henri Poincaré, Probabilités et Statistiques* (2019), vol. 55, Institut Henri Poincaré, pp. 184–210.
- [41] HINTON, G., DENG, L., YU, D., DAHL, G. E., MOHAMED, A.-R., JAITLEY, N., SENIOR, A., VANHOUCHE, V., NGUYEN, P., SAINATH, T. N., AND KINGSBURY, B. Deep Neural Networks for Acoustic Modeling in Speech Recognition: The Shared Views of Four Research Groups. *IEEE Signal Processing Magazine* 29, 6 (2012), 82–97.
- [42] HOCHBRUCK, M., AND OSTERMANN, A. Explicit exponential Runge-Kutta methods for semilinear parabolic problems. *SIAM J. Numer. Anal.* 43, 3 (2005), 1069–1090.
- [43] HSIEH, J.-T., ZHAO, S., EISMANN, S., MIRABELLA, L., AND ERMON, S. Learning Neural PDE Solvers with Convergence Guarantees. *arXiv:1906.01200* (2019).
- [44] HUANG, R., LI, R., AND XI, Y. Learning Optimal Multigrid Smoothers via Neural Networks. *SIAM Journal on Scientific Computing* 45, 3 (2023), S199–S225.
- [45] HUANG, Z., LIANG, S., ZHANG, H., YANG, H., AND LIN, L. On fast simulation of dynamical system with neural vector enhanced numerical solver. *Scientific Reports* 13, 1 (Sep 2023), 15254.
- [46] HUTZENTHALER, M., JENTZEN, A., KRUSE, T., NGUYEN, T. A., AND VON WURSTEMBERGER, P. Overcoming the curse of dimensionality in the numerical approximation of semilinear parabolic partial differential equations. *Proc. A.* 476, 2244 (2020), 20190630, 25.
- [47] JENTZEN, A., KUCKUCK, B., AND VON WURSTEMBERGER, P. Mathematical Introduction to Deep Learning: Methods, Implementations, and Theory. *arXiv:2310.20360* (2023).
- [48] JOVANOVIĆ, B. S., AND SÜLI, E. *Analysis of Finite Difference Schemes*. Springer London, 2014.
- [49] KARNIADAKIS, G. E., KEVREKIDIS, I. G., LU, L., PERDIKARIS, P., WANG, S., AND YANG, L. Physics-informed machine learning. *Nature Reviews Physics* 3, 6 (2021), 422–440.
- [50] KATRUTSA, A., DAULBAEV, T., AND OSELEDETS, I. Deep Multigrid: learning prolongation and restriction matrices. *arXiv:1711.03825* (2017).
- [51] KHOO, Y., LU, J., AND YING, L. Solving parametric PDE problems with artificial neural networks. *European J. Appl. Math.* 32, 3 (2021), 421–435.
- [52] KOCHKOV, D., SMITH, J. A., ALIEVA, A., WANG, Q., BRENNER, M. P., AND HOYER, S. Machine learning-accelerated computational fluid dynamics. *Proc. Natl. Acad. Sci. USA* 118, 21 (2021), Paper No. e2101784118, 8.

- [53] KOSSACZKÁ, T., EHRHARDT, M., AND GÜNTHER, M. Deep FDM: Enhanced finite difference methods by deep learning. *Franklin Open* 4 (2023), 100039.
- [54] KOVACHKI, N., LANTHALER, S., AND MISHRA, S. On universal approximation and error bounds for Fourier neural operators. *J. Mach. Learn. Res.* 22 (2021), Paper No. [290], 76.
- [55] KRIZHEVSKY, A., SUTSKEVER, I., AND HINTON, G. E. ImageNet Classification with Deep Convolutional Neural Networks. In *Advances in Neural Information Processing Systems* (2012), F. Pereira, C. Burges, L. Bottou, and K. Weinberger, Eds., vol. 25, Curran Associates, Inc.
- [56] LANTHALER, S., MOLINARO, R., HADORN, P., AND MISHRA, S. Nonlinear reconstruction for operator learning of PDEs with discontinuities. *arXiv:2210.01074* (2022).
- [57] LEVEQUE, R. J. *Finite Difference Methods for Ordinary and Partial Differential Equations*. Society for Industrial and Applied Mathematics, 2007.
- [58] LI, Z., HUANG, D. Z., LIU, B., AND ANANDKUMAR, A. Fourier neural operator with learned deformations for PDEs on general geometries. *arXiv:2207.05209* (2022).
- [59] LI, Z., KOVACHKI, N., AZIZZADENESHELI, K., LIU, B., BHATTACHARYA, K., STUART, A., AND ANANDKUMAR, A. Neural operator: Graph kernel network for partial differential equations. *arXiv:2003.03485* (2020).
- [60] LI, Z., KOVACHKI, N., AZIZZADENESHELI, K., LIU, B., BHATTACHARYA, K., STUART, A., AND ANANDKUMAR, A. Fourier neural operator for parametric partial differential equations. In *International Conference on Learning Representations* (2021).
- [61] LIST, B., CHEN, L.-W., AND THUREY, N. Learned turbulence modelling with differentiable fluid solvers: physics-based loss functions and optimisation horizons. *Journal of Fluid Mechanics* 949 (2022), A25.
- [62] LIU, Y., KUTZ, J. N., AND BRUNTON, S. L. Hierarchical deep learning of multiscale differential equation time-steppers. *Philos. Trans. Roy. Soc. A* 380, 2229 (2022), Paper No. 20210200, 17.
- [63] LU, L., JIN, P., PANG, G., ZHANG, Z., AND KARNIADAKIS, G. E. Learning nonlinear operators via DeepONet based on the universal approximation theorem of operators. *Nat. Mach. Intell.* 3, 3 (2021), 218–229.
- [64] LU, L., MENG, X., CAI, S., MAO, Z., GOSWAMI, S., ZHANG, Z., AND KARNIADAKIS, G. E. A comprehensive and fair comparison of two neural operators (with practical extensions) based on fair data. *Computer Methods in Applied Mechanics and Engineering* 393 (2022), 114778.
- [65] MAULIK, R., SAN, O., RASHEED, A., AND VEDULA, P. Subgrid modelling for two-dimensional turbulence using neural networks. *Journal of Fluid Mechanics* 858 (2019), 122–144.
- [66] MEHRISH, A., MAJUMDER, N., BHARDWAJ, R., MIHALCEA, R., AND PORIA, S. A review of deep learning techniques for speech processing. *arXiv:2305.00359* (2023).
- [67] MISHRA, S. A machine learning framework for data driven acceleration of computations of differential equations. *Math. Eng.* 1, 1 (2019), 118–146.
- [68] NELSEN, N. H., AND STUART, A. M. The random feature model for input-output maps between Banach spaces. *SIAM J. Sci. Comput.* 43, 5 (2021), A3212–A3243.
- [69] NGUWI, J. Y., PENENT, G., AND PRIVAULT, N. A fully nonlinear Feynman-Kac formula with derivatives of arbitrary orders. *arXiv:2201.03882* (2022).
- [70] NOVAK, E., AND WOŹNIAKOWSKI, H. *Tractability of Multivariate Problems: Standard information for functionals*, vol. 12. European Mathematical Society, 2008.

- [71] NOVAK, E., AND WOŹNIAKOWSKI, H. *Tractability of multivariate problems. Vol. 1: Linear information*, vol. 6 of *EMS Tracts in Mathematics*. European Mathematical Society (EMS), Zürich, 2008.
- [72] OPENAI. GPT-4 Technical Report. *arXiv:2303.08774* (2023).
- [73] OUALA, S., DEBREU, L., PASCUAL, A., CHAPRON, B., COLLARD, F., GAULTIER, L., AND FABLET, R. Learning Runge-Kutta integration schemes for ODE simulation and identification. *arXiv:2105.04999* (2021).
- [74] PAZY, A. *Semigroups of linear operators and applications to partial differential equations*, vol. 44 of *Applied Mathematical Sciences*. Springer-Verlag, New York, 1983.
- [75] PHAM, H., AND WARIN, X. Mean-field neural networks: learning mappings on Wasserstein space. *arXiv:2210.15179* (2022).
- [76] QIU, X., SUN, T., XU, Y., SHAO, Y., DAI, N., AND HUANG, X. Pre-trained models for natural language processing: A survey. *Science China Technological Sciences* 63, 10 (Sept. 2020), 1872–1897.
- [77] RAISSI, M., PERDIKARIS, P., AND KARNIADAKIS, G. E. Physics-informed neural networks: a deep learning framework for solving forward and inverse problems involving nonlinear partial differential equations. *J. Comput. Phys.* 378 (2019), 686–707.
- [78] RAONIĆ, B., MOLINARO, R., ROHNER, T., MISHRA, S., AND DE BEZENAC, E. Convolutional Neural Operators. *arXiv:2302.01178* (2023).
- [79] RAY, D., AND HESTHAVEN, J. S. An artificial neural network as a troubled-cell indicator. *Journal of Computational Physics* 367 (2018), 166–191.
- [80] ROGERS, A., KOVALEVA, O., AND RUMSHISKY, A. A primer in BERTology: What we know about how BERT works. *Transactions of the Association for Computational Linguistics* 8 (2020), 842–866.
- [81] SAN, O., AND MAULIK, R. Extreme learning machine for reduced order modeling of turbulent geophysical flows. *Phys. Rev. E* 97 (Apr 2018), 042322.
- [82] SCIPY DEVELOPERS. Scipy reference guide: Rbfinterpolator, 2021.
- [83] SELL, G. R., AND YOU, Y. *Dynamics of evolutionary equations*, vol. 143 of *Applied Mathematical Sciences*. Springer-Verlag, New York, 2002.
- [84] SHEN, X., CHENG, X., AND LIANG, K. Deep Euler method: solving ODEs by approximating the local truncation error of the Euler method. *arXiv:2003.09573* (2020).
- [85] SIRIGNANO, J., AND SPILIOPOULOS, K. DGM: A deep learning algorithm for solving partial differential equations. *Journal of Computational Physics* 375 (2018), 1339–1364.
- [86] SUBEL, A., CHATTOPADHYAY, A., GUAN, Y., AND HASSANZADEH, P. Data-driven subgrid-scale modeling of forced Burgers turbulence using deep learning with generalization to higher Reynolds numbers via transfer learning. *Physics of Fluids* 33, 3 (Mar. 2021).
- [87] TADMOR, E. A review of numerical methods for nonlinear partial differential equations. *Bull. Amer. Math. Soc. (N.S.)* 49, 4 (2012), 507–554.
- [88] THOMÉE, V. *Galerkin finite element methods for parabolic problems*, second ed., vol. 25 of *Springer Series in Computational Mathematics*. Springer-Verlag, Berlin, 2006.
- [89] TOMPSON, J., SCHLACHTER, K., SPRECHMANN, P., AND PERLIN, K. Accelerating Eulerian fluid simulation with convolutional networks. In *Proceedings of the 34th International Conference on Machine Learning* (06–11 Aug 2017), D. Precup and Y. W. Teh, Eds., vol. 70 of *Proceedings of Machine Learning Research*, PMLR, pp. 3424–3433.

- [90] TSITOURAS, C. Neural networks with multidimensional transfer functions. *IEEE Transactions on Neural Networks* 13, 1 (2002), 222–228.
- [91] VASWANI, A., SHAZEER, N., PARMAR, N., USZKOREIT, J., JONES, L., GOMEZ, A. N., KAISER, L. U., AND POLOSUKHIN, I. Attention is All you Need. In *Advances in Neural Information Processing Systems* (2017), I. Guyon, U. V. Luxburg, S. Bengio, H. Wallach, R. Fergus, S. Vishwanathan, and R. Garnett, Eds., vol. 30, Curran Associates, Inc.
- [92] VOULODIMOS, A., DOULAMIS, N., DOULAMIS, A., AND PROTOPAPADAKIS, E. Deep Learning for Computer Vision: A Brief Review. *Computational Intelligence and Neuroscience 2018* (2018), 1–13.
- [93] WANG, Y.-J., AND LIN, C.-T. Runge-Kutta neural network for identification of dynamical systems in high accuracy. *IEEE Transactions on Neural Networks* 9, 2 (1998), 294–307.
- [94] YU, D., AND DENG, L. *Automatic Speech Recognition: A Deep Learning Approach*. Springer London, 2015.
- [95] ZHU, Y., AND ZABARAS, N. Bayesian deep convolutional encoder-decoder networks for surrogate modeling and uncertainty quantification. *J. Comput. Phys.* 366 (2018), 415–447.